Titre: Title:	Thermodynamic and Kinetic Modeling of Thermal Decarbonization of Low-Grade Phosphate Ore
Auteur: Author:	Hassan Gezzaz
Date:	2021
Type:	Mémoire ou thèse / Dissertation or Thesis
Référence: Citation:	Gezzaz, H. (2021). Thermodynamic and Kinetic Modeling of Thermal Decarbonization of Low-Grade Phosphate Ore [Mémoire de maîtrise, Polytechnique Montréal]. PolyPublie. https://publications.polymtl.ca/9960/

POLYTECHNIQUE MONTRÉAL

affiliée à l'Université de Montréal

Thermodynamic and Kinetic Modeling of Thermal Decarbonization of Low-grade Phosphate ore

HASSAN GEZZAZ

Département de génie chimique

Mémoire présenté en vue de l'obtention du diplôme de *Maîtrise ès sciences appliquées*

Génie chimique

Décembre 2021

POLYTECHNIQUE MONTRÉAL

affiliée à l'Université de Montréal

Ce mémoire intitulé :

Thermodynamic and Kinetic Modeling of Thermal Decarbonization of Low-grade Phosphate ore

présenté par **Hassan GEZZAZ**

en vue de l'obtention du diplôme de *Maîtrise ès sciences appliquées*

a été dûment accepté par le jury d'examen constitué de :

Jean-Philippe HARVEY, président

Jamal CHAOUKI, membre et directeur de recherche

Redouane BENI AZZA, membre

ACKNOWLEDGEMENTS

I would first like to express my heartfelt thanks to my supervisor, Professor Jamal Chaouki, for his support, trust, and encouragement during all these past years. His competent help and confidence enabled me to successfully complete this master project and acquire the required knowledge to conduct a research project.

Special thanks go to Mohammad Latifi for his help, support, and guidance. I also would like to thank Said Samih for his help and support during his studies at Polytechnique Montreal. I would like to thank the technicians Sylvain, Rafael, and Maxime, as well as the administrative staff of the department of chemical engineering, particularly Brigitte. I am deeply thankful to the members of Professor Jamal Chaouki's group, Mitra, Ahmad-Reza, and Eltefat who helped me in this project. The achievement of this thesis would not have been possible without their pleasant support and guidance. Thanks to Afshin, who was always available to help me for characterization with ICP-OES. I would like to warmly thank Polytechnique Montreal and OCP group for the financial support and available resources for this project.

Finally, I would like to sincerely thank my family, for their encouragement, wishes, sacrifices, and support during my studies.

RÉSUMÉ

Le minerai de phosphate est une source potentielle de phosphore avec une large application dans de nombreux procédés industriels pour produire des produits commerciaux tels que l'acide phosphorique, les aliments, les engrais, les pesticides et les détergents. Le minerai de phosphate est une roche naturelle contenant principalement la fluorapatite carbonée, la dolomite, la calcite et le quartz.

Le minerai de phosphate à faible teneur est bénéfique pour produire du gaz phosphore pur (P_2) par fusion, car il contient une concentration importante de quartz qui joue le rôle d'un agent fondant. Le gaz phosphore peut être transformé en d'autres produits intermédiaires purs tels que le pentoxyde de phosphore (P_2O_5) et l'acide phosphorique (H_3PO_4), qui ont un large éventail d'applications industrielles. Par conséquent, le procédé thermique par fusion est une technique prometteuse pour remplacer le procédé à l'acide phosphorique humide qui souffre de nombreux problèmes techniques (acide phosphorique de faible teneur) et cause de graves problèmes environnementaux (génération de phosphogypse).

L'objectif de ce projet de recherche est d'étudier la décarbonisation thermique du minerai de phosphate à faible teneur (25-1000 ºC) en tant que technique de valorisation appropriée pour éliminer le carbone contenu dans le minerai de phosphate avant la production de P_2 par procédé de fusion.

Le présent travail de recherche vise à : i) effectuer une analyse thermodynamique détaillée de la décarbonisation thermique du minerai de phosphate à faible teneur avec Factsage^{TM}, ii) optimiser les conditions opérationnelles expérimentales pour éliminer le carbone du minerai de phosphate à faible teneur par traitement thermique et suivre la transformation des phase cristallines à différentes

étapes (XRD, LECO) et pour valider la distribution de ces phases cristallines à l'aide l'analyse thermodynamique, iii) effectuer une analyse cinétique de la décarbonisation thermique du minerai de phosphate à faible teneur avec une analyse thermogravimétrique dans des conditions non isothermes en couplant des méthodes isoconversionelles (OFW, KAS , Starink, Vyazovkin) et les méthodes d'ajustement du modèle (équation de Coats-Redfern). La séquence de réactions de décarbonisation thermique du minerai de phosphate à faible teneur a été proposée en combinant les résultats de la caractérisation, de l'analyse thermodynamique et de la modélisation cinétique.

L'analyse thermodynamique et l'analyse avec XRD-LECO ont montré que la carbonate-fluorapatite ($Ca_{9.55}(PO_4)_{4.96}F_{1.96}(CO_3)_{1.283}$), la calcite ($CaCO_3$) et la dolomite ($CaMg(CO_3)_2$) se décomposent en dioxyde de carbone et en nouveaux produits, notamment l'oxyde de calcium (CaO) et l'oxyde de magnésium (MgO) qui réagissent avec le quartz (SiO_2) pour former des silicates de magnésium (Mg_2SiO_4), des silicates de calcium (Ca_2SiO_4) et des silicates de calcium-magnésium ($CaMgSi_2O_6$).

La combinaison de méthodes isoconversionnelles et de méthodes modèlistiques a montré que la décarbonisation thermique du minerai de phosphate à faible teneur est un procédé à plusieurs étapes à cause de l'hétérogénéité du phosphate à faible teneur. Par conséquent, les paramètres cinétique (modèle de mécanisme de réaction, énergie d'activation, facteur pré-exponentiel) ont été fournis pour chaque étape. Les énergies d'activation calculées ont été utilisées comme caractéristique de réaction pour confirmer la décomposition de minéraux carbonés (fluorapatite carbonée, calcite, dolomite). Cette hypothèse est valable lorsque la réactivité des matériaux n'affecte pas significativement le comportement cinétique des systèmes. Les énergies d'activation obtenues pour chaque étape sont en accord avec celles des études antérieures rapportées dans la littérature, ce qui

valide la fiabilité de l'approche appliquée (approche de déconvolution mathématique, fonction d'ajustement de plusieurs pics, et techniques pour déterminer les conversions de réactions d'individuelles).

ABSTRACT

Phosphate ore is a potential source of phosphorus with wide application in many industrial processes to produce market products such as phosphoric acid, food, fertilizers, pesticides, and detergents. It is a natural rock that contains mainly carbonate fluorapatite, dolomite, calcite, and quartz.

Low-grade phosphate ore is beneficial to produce high pure phosphorus gas (P_2) by smelting process because it contains a considerable concentration of quartz that plays the role of fluxing agent. Phosphorus gas can be transformed into other pure intermediate products such as phosphorus pentoxide (P_2O_5) and phosphoric acid (H_3PO_4), which have a wide range of industrial applications. Hence, the thermal process that includes smelting is a promising technique to replace the wet phosphoric acid process that suffers from many technical issues (low-grade phosphoric acid) and causes serious environmental problems (generation of phosphogypsum).

This research project was aimed to study the thermal decarbonization of low-grade phosphate ore (25-1000 ºC) as an appropriate upgrading technique to remove carbon from the low-grade phosphate ore before the production of gaseous P_2 by smelting process.

The present research work aims to: i) perform a detailed thermodynamic analysis of thermal decarbonization of low-grade phosphate ore with Factsage^{TM}, ii) optimize experimental operational conditions to remove carbon from low-grade phosphate ore by heat treatment, and track the phase transformation at different stages (XRD, LECO) and validate the crystalline phase distribution with help of thermodynamic analysis, iii) perform kinetic analysis of thermal decarbonization of low-grade phosphate ore with thermogravimetric analysis under non-isothermal conditions by coupling isoconversional methods (OFW, KAS, Starink, Vyazovkin) and model fitting methods

(Coats-Redfern Equation). A plausible reaction pathway of thermal decarbonization of low-grade phosphate ore was proposed by combining the results of characterization, thermodynamic analysis, and kinetic modeling.

Thermodynamic analysis and XRD-LECO analysis showed that carbonate-fluorapatite ($Ca_{9.55}(PO_4)_{4.96}F_{1.96}(CO_3)_{1.283}$), calcite ($CaCO_3$) and dolomite ($CaMg(CO_3)_2$) are decomposed to carbon dioxide and new products including calcium oxide (CaO) and magnesium oxide (MgO) that reacted with quartz (SiO_2) to form magnesium silicate (Mg_2SiO_4), calcium silicates (Ca_2SiO_4) and calcium-magnesium silicates ($CaMgSi_2O_6$).

The combination of isoconversional methods and model-free methods demonstrated that the thermal decarbonization of low-grade phosphate ore is a multi-step reaction process due to the heterogeneity of low-grade phosphate ore. Therefore, the triple-kinetic parameters (reaction mechanism model, activation energy, pre-exponential factor) were provided for each step. The calculated activation energies were used as a reaction characteristic to confirm the occurrence of decomposition carbon-bearing minerals. This assumption is valid when the reactivity of the materials does not significantly affect the kinetic behaviour of systems. The activation energies obtained for each step were quite consistent with the data reported in the literature.

TABLE OF CONTENTS

LIST OF TABLES

LIST OF FIGURES

LIST OF ABBREVIATIONS

A	Pre-exponential factor
BET	Brunauer–Emmett–Teller
BPL	Bone Phosphate of lime
$Ca_{10}(PO_4)_6(Cl)_2$	Chlorapatite
$Ca_{10}(PO_4)_6(OH)_2$	Hydroxyapatite
$Ca_{10}(PO_4)_6F_2$	Fluorapatite
Ca_2SiO_4	Dicalcium silicates
$Ca_3(PO_4)_2$	Tricalcium phosphate
$Ca_{9.55}(PO_4)_{4.96}F_{1.96}(CO_3)_{1.283}$	Carbonate-fluorapatite
$CaCO_3$	Calcite
$CaMg(CO_3)_2$	Dolomite
$CaMgSi_2O_6$	Diopside
CaO	Calcium oxide
$CaSiO_3$	Monocalcium silicates
CO	Carbon monoxide
CO_2	Carbon dioxide
CO_3^{2-}	Carbonate ions

DSC	Differential Scanning Calorimetry
DTG	Derivative Thermogravimetry
dX/dt	Reaction rate
Ea	Activation energy
f(X)	Differential reaction model
FeP_2	Ferrophosphorus
FTIR	Fourier-Transform Infrared Spectroscopy
FWO	Flynn–Wall–Ozawa
g(X)	Integral reaction model
H_2SO_4	Sulfuric acid
H_3PO_4	Phosphoric acid
HVL	Haarhoff-Van der Linde
ICP-OES	Inductively coupled plasma optical emission spectroscopy
ICSD	Inorganic Crystal Structure Database
ICTAC	International Confederation for Thermal Analysis and Calorimetry
KAS	Kissinger–Akahira–Sunose
KAS	Kissinger-Akahira-Sunose
Mg_2SiO_4	Forsterite

$MgCO_3$	Magnesite
MgO	Magnesium oxide
N2	Nitrogen
P_2	Phosphorus gas
P_2O_5	Phosphorus pentoxide
PO_4^{3-}	Orthophosphate ions
R	Gas constant
R^2	Correlation coefficient
RSS	Residual sum of squares
RT	Room temperature
SAF	Submerged arc furnace
SiO_2	Quartz/Silica
TGA	Thermogravimetry analysis
WPPA	Wet Phosphoric Acid Process
XRD	X-Ray Diffraction
β	Heating rate

LIST OF APPENDICES

CHAPTER 1 INTRODUCTION

1.1 Problem statement and motivations

Phosphorus is the eleventh most abundant element in the earth's crust, i.e., 0.1 wt% [1]. This non-renewable source is the third macronutrient for life in addition to nitrogen and potassium [2, 3]. Phosphorus is a potential element with a wide range of applications in many industrial processes to produce market products such as phosphoric acid, food/nutrition products, fertilizers, pesticides, metal treatment, and detergents. It is naturally combined with other elements such as calcium and oxygen in the form of apatite minerals (e.g., fluorapatite, hydroxyapatite, chlorapatite) in phosphate ore matrix [4].

Fertilizers manufactory consumes around 85% of mined phosphate ore worldwide [5]. Due to its economic feasibilities, Wet Phosphoric Acid Process (WPPA) using sulfuric acid (H_2SO_4) is the widespread technique to produce H_3PO_4 which is then transformed into fertilizers. Nevertheless, the thermal process represents an excellent opportunity to overcome problems encountered in WPPA, which include generation of phosphogypsum as a by-product, accumulation of cadmium in phosphoric acid, and requirement of high-grade phosphate ore (>35% P_2O_5) to produce H_3PO_4 [6-10]. Moreover, unlike WPPA, which is limited to the direct production of phosphoric acid used only for fertilizers production, the thermal process allows the production of a series of pure intermediates products, $P_2(g)$, $P_2O_5(s)$, and H_3PO_4 through the three steps. These phosphorus derivatives have a wide range of applications to manufacturing various market products that require high purity of phosphorus [11, 12]. In the first stage of the thermal process, fluorapatite reacts with silica (SiO_2) as a fluxing agent and a reducing agent to produce gaseous phosphorus (P_2), carbon monoxide (CO), and complex slag [13]. This endothermic reaction is called carbothermal reduction

or smelting. It occurs at very high temperatures 1200-1500 ° C, depending on basicity (CaO/SiO_2) and C/P_2O_5 ratios. The gaseous product P_2 can be then burnt with oxygen to form P_2O_5, which reacts with water to form H_3PO_4.

Smelting of phosphate ore to produce P_2 is the core step of the thermal process to manufacture a highly pure phosphoric acid. Previous bench-scale studies emphasized studying mechanisms and kinetics of smelting of phosphate ore and improving the operational conditions to optimize the conversion of P_2 [13-29], ignoring the improvement of other process features that must be considered for a successful scale-up to the industrial level. The production of P_2 in a single reactor at an industrial scale without appropriate beneficiation of phosphate ore, especially when dealing with low-grade phosphate ore (P_2O_5 below 20-25%) [30], may not be a good option for many reasons that will be highlighted in the next paragraphs.

Phosphate ore is a heterogeneous rock that can contain many mineral gangues such as calcite ($CaCO_3$) and dolomite ($CaMg(CO_3)_2$) depending on the origin [31]. $CaCO_3$ is decomposed via a single endothermic reaction into calcium oxide (CaO) and carbon monoxide (CO_2) at 800-1000 °C [9, 32, 33]. Similarly, $CaMg(CO_3)_2$, which contains $CaCO_3$ and $MgCO_3$, is decomposed through two steps into magnesium oxide (MgO), CaO, and CO_2 at 490-880 °C depending on the reaction atmosphere and heating rate [34, 35]. These reactions can occur during the smelting of phosphate ore. If the surface of the reducing agent is exposed to the released CO_2 from the thermal decomposition of carbonate minerals, the famous backward of Boudouard reaction, which is thermodynamically favorable at T>680°C, may occur [36, 37]. This reaction would result in a loss of carbon source before that smelting begins, which requires an excess of carbon source and thus

increases the cost of the process. Therefore, it is deemed to be reasonable to decarbonize low-grade phosphate ore before smelting.

The low-grade phosphate ore used in this research project was selected because it contains a considerable amount of quartz that plays the role of a fluxing agent in smelting process. However, it contains a considerable concentration of carbon-bearing minerals such as calcite, dolomite, and carbonate-fluorapatite. Therefore, to alleviate the impact of the problems discussed above, it is crucial to decarbonize low-grade phosphate ore before the smelting process to produce a highly pure P_2(g) and reduce the operational costs to ensure the long-term feasibility. Defluorination of phosphate ore at 1000-1100 °C [38] is a side advantage of the thermal decarbonization process. This option delivers the best technology for the sustainable economic feasibility of the overall process.

In the present research study, the thermal decarbonization of low-grade phosphate ore was suggested as a pre-treatment step of the smelting process. The thermodynamic and kinetics of thermal decarbonization of low-grade phosphate ore were studied. Moreover, the operational conditions were optimized for the removal of carbon from carbon-bearing minerals.

Extensive research works were published on the thermal beneficiation of phosphate ore. The researchers focused on the decomposition of calcite and dolomite. However, they ignored the thermal behaviour of carbonate fluorapatite that may undergo a transformation during the process. Phosphate ore tested in literature contains fluorapatite as a phosphorus-bearing mineral instead of carbonate fluorapatite. However, phosphate ore used in the present study contains carbonate fluorapatite, which may make a new challenge to remove carbon from all carbon-bearing minerals

forming phosphate ore. Therefore, it was aimed to investigate the transformation of this mineral at decarbonization temperatures and achieve the maximal removal of carbon.

To our knowledge, no thermodynamic analysis study of thermal decarbonization of phosphate ore study has been conducted. Moreover, although the kinetics of thermal decomposition of phosphate ore has been studied, the complex heterogeneity of the low-grade phosphate ore used in the present study stimulated to provide the corresponding kinetics parameters relevant to the characteristics of the ore, particularly in the presence of carbonate-fluorapatite. Such analysis enabled to mitigate uncertainties for eventual process design. Kinetics of thermal decarbonization of low-grade phosphate ore will play an essential role in the design and optimization of the reactor. However, the kinetic parameters must be estimated accurately.

1.2 Research objectives

Low-grade phosphate ore accommodates three carbon-bearing minerals, namely carbonate fluorapatite, calcite, and dolomite. These minerals must exhibit a thermal treatment to liberate carbon from their structures. The decarbonized phosphate is then directed to a smelting reactor to produce P_2. The main objective of this study is to study the thermal decarbonization of low-grade phosphate ore by combining thermodynamics, characterization, and kinetic modeling. Low-grade phosphate ore is subjected to high temperatures 700-1000 °C to decarbonize carbon-bearing minerals.

The first step is to maximize the removal of carbon and investigate the mineralogy of the decarbonized phosphate with characterization and thermodynamic analysis. The second step is to model the kinetics with thermogravimetry analysis.

The suggested sub-objectives are as follow:

- Sub-objective 1: Thermodynamic analysis of thermal decarbonization of low-grade phosphate ore with Factsage^{TM}.
- Sub-objective 2: Optimize experimentally operating conditions for the removal of carbon from low-grade phosphate ore by thermal treatment and investigate the thermal behaviour of carbonate-fluorapatite.
- Sub-objective 3: Kinetic modeling of thermal decarbonization of low-grade phosphate ore with thermogravimetry analysis.

CHAPTER 2 LITERATURE REVIEW

2.1 Mineralogy of phosphate ore

Phosphate ore is the primary source of phosphorus. There are two main types of phosphate ore: sedimentary deposits and igneous deposits. Sedimentary deposits are high-grade ores (18-35% P_2O_5) occurring in marine mediums and represent 80% of the global reserves. Igneous deposits are metamorphic ores resulted from melt cooling. Igneous deposits are less pure compared to sedimentary deposits containing less than 15% of P_2O_5. Phosphorus element is incorporated in phosphate ore as apatite (fluorapatite ($Ca_{10}(PO_4)_6F_2$), chlorapatite ($Ca_{10}(PO_4)_6(Cl)_2$), and hydroxyapatite ($Ca_{10}(PO_4)_6(OH)_2$)). Heterogeneous phosphate ore is formed from the association of apatite and other minerals such as calcite, dolomite, clays, and quartz. The concentration of minerals varies from a location to another depending on the quality of phosphate ore. Table 2-1 shows a typical mineral and chemical composition of phosphate ore from different countries.

Fluorapatite ($Ca_{10}(PO_4)_6F_2$) is traditionally formed in igneous deposits but also sedimentary deposits. It exhibits particularly many ionic substitutions in its crystal lattice, which gives it the general formula $Ca_{10-x-y}Na_xMg_y(PO_4)_{6-z}(CO_3)_zF_{0.4z}F_2$ [31]. The cationic substitutions of Ca^{2+} by Na^+ or Mg^{2+} and anionic substitutions of complex ions of phosphates by carbonate ions must result from electric charge and ionic radii. The penetration of carbonate ions in fluorapatite structure results in the formation of carbonate-fluorapatite.

Table 2-1 Mineral and chemical composition of phosphate ore in some worldwide deposits

Country	Type of ore	Mineral composition (%)						Chemical composition								
		Apatite	Calcite	Dolomite	Quartz	Feldspar	Clay	P_2O_5	CaO	MgO	SiO_2	Al_2O_3	TiO_2	Fe_2O_3	Na_2O	F
Morocco [39]	Sedimentary	90	2.6	1.8	1.4	-	1.2	31.51	50.19	0.84	2.45	0.30	-	0.15	0.84	3.82
China [40]	Sedimentary	52.5	-	10.3	16.3	-	-	21.54	31.77	2.24	25.2	4.56	-	2.3	-	-
United States (FLORIDA) [41]	Sedimentary	-	-	-	-	-		33.34	48.02	0.325.5	1.3		-	1.08	-	-
akhstan[42]	Igneous	-	-	-	-	-	-	23.5	40	4.2	13.7	-	-	-	-	-
Tunisia [43]	Sedimentary	High	Low	Low	Low	-	-	29.58	49.45	0.7	3.08	0.86	-	0.25	1.39	2.84
Russia [44]	Igneous	-	-	-	-			12.50	18.28	0.92	32.5	15.52	2.20	5.45	5.56	-
Greece [45]	Sedimentary	High	Medium	Low	Medium	Low	-	21.97	39.72	1.74	11.7	1.96	0.12	3.60	1.15	2.35

2.2 Smelting of phosphate ore to produce gaseous phosphorus

The smelting process is the technology employed to produce P_2 by mixing phosphate ore, fluxing agent, and reducing agent at controlled mass ratios of SiO_2/CaO and C/P_2O_5. The mixture is heated at specific temperatures (1200-1600 °C). The role of the fluxing agent is to reduce the slagging temperature of the system or form a eutectic system that transforms phosphorus-bearing minerals into molten phases P_2O_5 in a complex heterogenous slag, which is reduced by a carbon source to produce P_2. Many reactions have been proposed to illustrate smelting of phosphorus-bearing minerals ($Ca_{10}(PO_4)_6F_2$, $Ca_3(PO_4)_2$) to produce P_2 based on analytical techniques and thermodynamic analysis. The reactions of smelting discussed in previous research works can be classified into two main categories. Some researchers claimed that P_2 is generated from a solid-liquid interaction between slag containing phosphorus and carbon [13, 18, 19, 27].

Other researchers suggested that it is produced directly from a solid-solid interaction between phosphorus-bearing minerals and carbon [15, 19-22, 24, 27, 29]. Such discrepancy must be attributed to many factors such as the type of minerals, fluxing agent, reaction environment, the mass ratio of SiO_2/CaO, and analytical techniques. The smelting of phosphate ore is not the scope of the present study. However, the most recognized reaction for the smelting of fluorapatite with silica as fluxing agent is [13]:

$$Ca_{10}(PO_4)_6F_2(s) + 15C(s) + 9SiO_2(s) \rightarrow 3P_2(g) + 15CO(g) + 9CaO.SiO_2(slag) \quad (1)$$

Rotary kiln and submerged arc furnace are the two commonly used techniques to produce P_2. Rotary kilns are very popular reactors to produce phosphoric acid. Pellets prepared from a mixture of phosphate ore, silica, and coke, are fed from the top of the rotary kiln in a counter-current of hot gases produced from the combustion of natural gas. The rotary kiln consists of two zones. In the reducing zone, pellets generate phosphorus and other gases between 1200 and 1400 °C. The

generated high viscous silicate melts accumulate on the bottom. In the oxidizing region, the P_2 reacts with the oxidizing gases to release phosphorus pentoxide (P_2O_5), which is then absorbed by phosphoric acid at the output of the rotary kiln. The yielded phosphoric acid contains 70% of P_2O_5. The exhaust gases enter a scrubber to remove fluorine compounds. Figure 2-1 shows a typical schematic of the kiln phosphoric acid process. The heat released by exothermic combustion can preheat pellets, which reduces natural gas consumption. Moreover, P_2 and P_2O_5 are produced in a single reactor, making the process more effective [25]. The complex nature of feed preparation, heavy beneficiation, and high maintenance of rotary kiln due to movable parts can make this process economically unattractive.

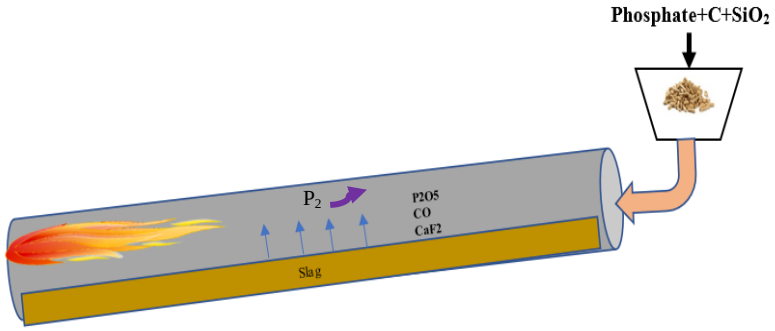

Figure 2-1 Schematic of Kiln Phosphoric Acid Process (Adapted from [25])

The submerged arc furnace (SAF) was extensively used in the last century to produce elemental phosphorus from phosphate ore. The crushed phosphate ore, silica, and carbon are pelletized in disk granulators to form uniform shapes with a size larger than 12.5 mm [39]. The mixture of phosphate ore, coke, and silica requires vigorous mixing before being smelted in SAF. The mixture is fed in the SAF, where arcs between the electrodes release heat. The electrical current in the SAF flows from the electrode toward the solid bed of the SAF (reactants) to generate heat and achieve a reaction temperature of 1200-1500 ºC. The molten slag and ferrophosphorus (FeP_2) accumulated

at the bottom of the furnace are evacuated from a casting hole. The gaseous products are directed upwards out of the SAF through sprayed outlets [39]. Figure 2-2 shows a depiction of SAF to produce phosphorus gas.

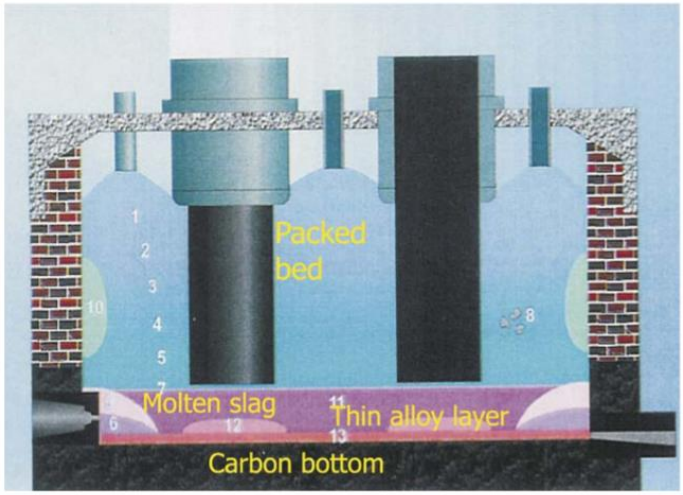

Figure 2-2 Schematic of Submerged Arc Furnace [39]

2.3 Thermal decomposition of phosphate ore

Calcination is a standard operation in which in which phosphate ore is heated at relatively high temperatures of 700-1000 °C depending on the quality of the deposit and the nature of impurities. The process consists of three main steps: i) moisture removal, ii) organic matter removal, and iii) liberation of carbon from the structure of calcite and dolomite, which are decomposed into their metal oxides and CO_2 (Equations 2,3). Calcination of dolomite and calcite is the most energy-consuming step of the process. Thermal decomposition is a crucial step to produce a commercial phosphate ore for the wet phosphoric acid process. Calcined phosphate accounts for about 10 % of world salable phosphate ore [9]. Sulfuric acid must be used in excess to produce H_3PO_4 which reacts with carbon and organic matter of phosphate ore if this latter is not decarbonized [40]. Furthermore, CO_2 can be generated causing the formation of foams that hinder the filtration of

phosphogypsum and H_3PO_4. Hence, thermal decomposition is a satisfactory technology to beneficiate phosphate ore and prepare it for any subsequent process that avoids the presence of carbon.

$$CaCO_3(s) \rightarrow CO_2(g) + CaO(s) \quad (2)$$

$$CaMg(CO_3)_2 \rightarrow CaO(s) + MgO(s) + 2CO_2(g) \quad (3)$$

Calcination of phosphate ore is a highly endothermic process consuming a large amount of energy because of the high heat required to dissociate carbonate minerals according to Equations 2 and 3. Calcination of typical phosphate ore with 50% $CaCO_3$ and 10% moisture consumes 3.6 GJ for each 1 ton of calcined product [9]. However, calcination can be an attractive solution if energy sources are sufficiently available to produce the energy at a relatively low cost [33].

Many inventions have been patented in the last decades to upgrade phosphate ore thermally and meet the requirements to produce high-grade wet phosphoric acid. In 1968, Haseman and coworkers of Armour Agricultural Chemical Co published a patent on the thermal beneficiation of phosphate ore very rich in carbonate minerals (dolomite and calcite) (>3% CO_2) [41]. The idea was to remove carbon contained in $CaCO_3$ and $CaMg(CO_3)_2$ that dissociate into CaO and MgO and CO_2 by calcination operation of 300 gram of phosphate ore at 900-2500 °F for 1 hour. To avoid the excess consumption of sulfuric acid, CaO and MgO can be eliminated by three operations: i) dedusting, ii) quenching followed by reaction with water to form insoluble slake products which decanted through a 150-mesh screen iii) dry grinding followed by air classification and then magnetic separation-air flotation to remove other impurities such as silicates. Dedusting was found to be more beneficial than hydration with water. It is desirable to eliminate magnesium from

phosphate ore because it can form an insoluble by-product in the fertilizers production process [42].

In another patent, Baumann and coworkers proposed a two-stage process that increases the concentration of P_2O_5 in sedimentary phosphate ore to the levels required to produce phosphoric acid and fertilizers (> 75-85 %) [43]. Phosphoric acid (P_2O_5 > 25%) with a controlled amount dilutes phosphate ore to increase the BPL (Bone Phosphate of lime) in the first step, and the product is then calcined at 450-1400 °F for further beneficiation. The first step is the best option to raise the concentration of BPL at the values required to produce superphosphate from phosphate ore with 75-85% of P_2O_5. However, the amount of Phosphoric acid must not be overestimated to avoid the formation of agglomerated sticky phosphate ore. Otherwise, upgraded phosphate ore can not be digested easily in the subsequent process of acidulation with sulfuric acid. The temperature range of calcination has been proposed to avoid particles sticking below 450 °F and prepare an easily grinded product, and design an energy-efficient process operating below 1400 °F.

Angevine and coworkers of Dorr-Olivier Incorporated developed a two-vessel fluidized bed system operating at high temperatures to give off CO_2 from carbonate minerals and cadmium of phosphate ore (Figure 2-3). The first vessel is devoted to the calcination of phosphate ore which does not require removal of cadmium. The vessel consists of three fluidized beds in which phosphate ore is firstly dried in the preheater at relatively low temperatures. The calciner fluidized bed operates at 735-785 °C under oxygen generated by a blower to oxidize organic matter and liberate carbon from dolomite and calcite of dried phosphate. Heat is supplied by fuel combustion. The retention time must be long enough for the complete liberation of CO_2 from organic matter and carbonate minerals. In the cooling-fluidized bed, the calcined phosphate is cooled at 120-540 °C, releasing

heat to the entering oxygen, which preheats phosphate ore in the dried/preheater fluidized bed. This multi-stage fluidized bed process is energetically efficient since the heat recovered from the cooling of calcined phosphate is captured for drying of phosphate ore. This first vessel is largely sufficient for volatilization of heavy metals such as cadmium which have sublimation temperature falling in the operational temperature of the calciner fluidized bed. The temperature of the calciner fluidized bed must be adjusted to 1000-1150 °C to cover the temperature of volatilization of cadmium. To hinder the circulating load of cadmium, Angevine and coworkers suggested addition of separate fluidized bed (second vessel) to remove cadmium after the calcination of dried phosphate ore in the first vessel. It is important to control the rate of oxygen in the second vessel since cadmium removal prefers neutral or reducing environments.

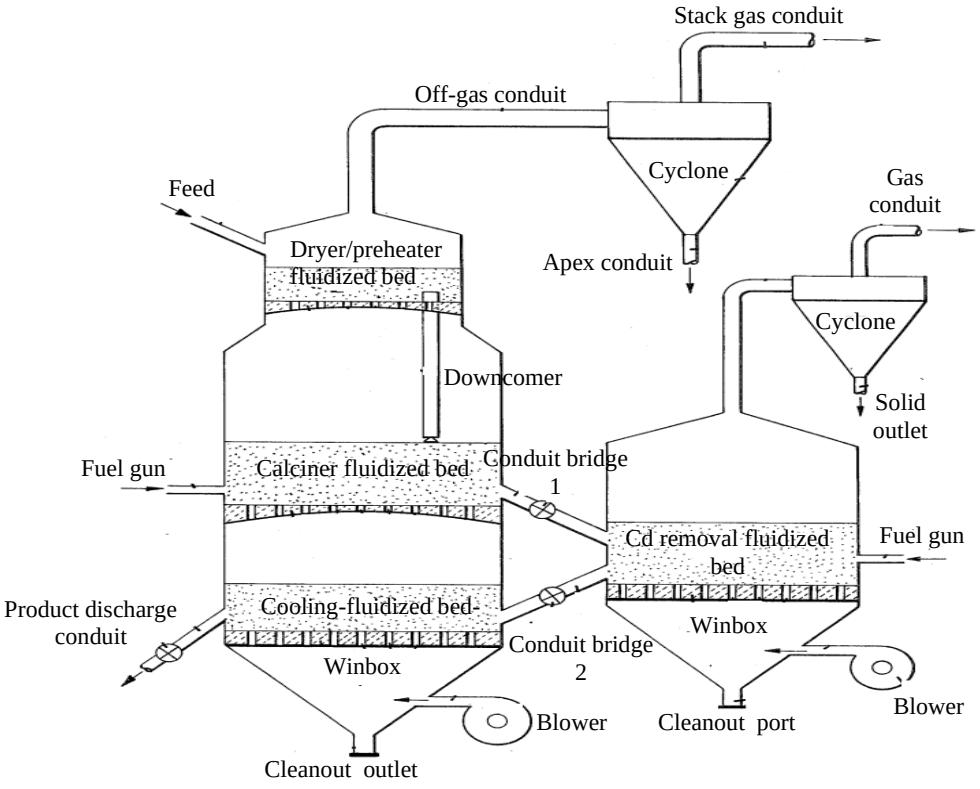

Figure 2-3 Fluidized bed for cadmium and harmful substances from phosphate ore by calcination [44]

It is worth noting that the processes discussed above were proposed to enhance the characteristics of phosphate ore by thermal route to meet the commercial requirement to produce specific products such as phosphoric acid superphosphate. For instance, silicates must not be eliminated during the thermal treatment of phosphate ore because of their role as a fluxing agent.

2.3.1 Impact of thermal decomposition on physical, chemical, and structural properties

Despite the numerous benefits of thermal decomposition of phosphate ore, it changes the physical, chemical, and structural characteristics of the treated phosphate ore. A vigorous control of these features helps to improve the efficiency of WPPA to produce high-grade phosphoric acid. However, relevant characteristics will be discussed to seek opportunities to improve the quality of treated phosphate ore for an efficient reactor design of the smelting process.

2.3.1.1 Specific surface area

Specific surface area is a crucial parameter that influences the rate of interfacial reactions. The kinetics of multi-components reactions is favored when sufficient sites are available for an ultimate contact between reactants. The higher surface, the faster the reaction.

One of the drawbacks of the thermal treatment of phosphate ore is the decrease of the surface area of the treated phosphate as temperature increases. This behaviour was observed by Freeman et al. [38], who investigated the effect of temperature on the surface area of calcined Moroccan and Utah phosphate. The tests were performed on a muffle furnace at isothermal conditions between 450 and 1150 °C for 30 min. The results of nitrogen adsorption measurements using Brunauer–Emmett–Teller (BET) showed a drastic decline of specific surface area between 450 and 800 °C for both rocks (Figure 2-4). This decrease results from the sintering of particles [45,

46], which is driven by a decrease in interfacial energy. It is worth noting that specific surface area decrease is compensated by the particle size increase because of the agglomeration of the solid. In the same trend, El Ouardi et al. [47] assumed that the specific surface area of calcined phosphate decreases significantly with time at T>700 °C. Mgaidi et al. [48] attributed the decrease of the normalized surface area of phosphate ore between 500 and 940°C to the sintering mechanism since the densification step was predominant at this range. However, the slight decrease below 500 °C was attributed to the elimination of organic matter. Controlling the change of specific surface area during calcination is important to optimize the production of P_2 during smelting.

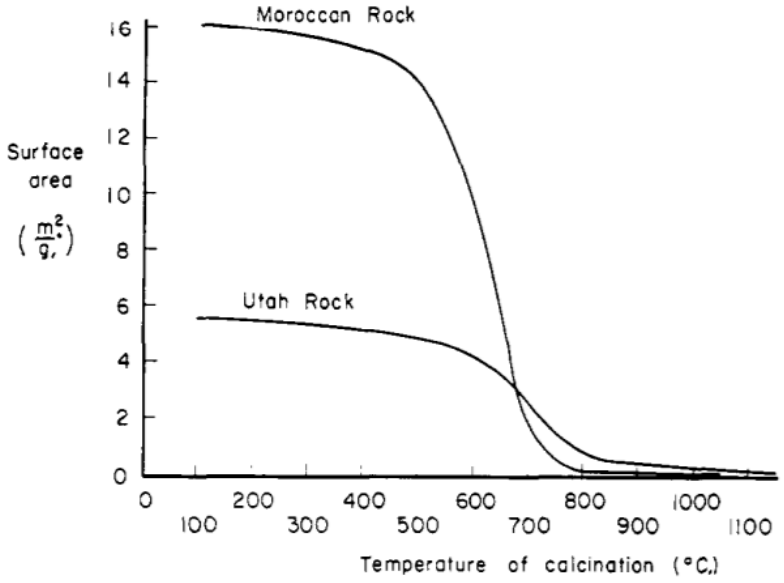

Figure 2-4 Effect of calcination temperature on specific surface area of Moroccan and Utah phosphate ore [38]

2.3.1.2 Porosity

Freeman et al. [38] found that porosity evolution with temperature depends on the phosphate ore quality. Under the same laboratory experimental conditions applied to investigate the change of specific surface area [38], the results demonstrated that the porosity decreased steadily with temperature for Moroccan phosphate ore. However, the porosity of Utah phosphate ore rose to 700 °C and then fell from this level. This behaviour was ascribed to the volatilization of organic matter present in Utah phosphate ore. The porosity decline may also result from sintering that tends to eliminate pores [49]. The control of the porosity is critical in thermal decomposition because it can affect the rate of external diffusion OF gas products such as CO_2. The rate of escape of CO_2 may be enhanced as the pores become wider.

2.3.1.3 Structural changes

Zhou et al. [50] performed their experiments on an electric tubular furnace at 600-1100 ºC under air atmosphere. They found that the content of P_2O_5, CaO, and MgO increased up to 950 ºC because of dolomite decarbonization. CaO and MgO then started to decrease from this temperature. They did not explain the reason behind the decrease in CaO and MgO content as they proposed in their reaction mechanisms. This decline may be attributed to the formation of calcium silicates ($CaSiO_3$) and magnesium silicates ($MgSiO_3$) as they proposed in their reaction mechanisms. Based on XRD data, the peaks of fluorapatite remained unchanged with temperature. Thermodynamic calculations performed by HSC 6.0 software confirmed that fluorapatite can not decompose nor react with quartz at the studied temperatures. These findings agree with those of Mgaidi et al. [48], who observed that adsorption peaks of the orthophosphate group PO_4^{3-} measured by IR spectrometry did not change at 940 °C. Recently, Chen et al. [51] studied the effect of temperature on the

structural changes of geological carbonate fluorapatite (C-Fap), synthetic hydroxyapatite (H-Ap), and bone bioapatite (B-Ap) between 100 and 900 ºC. Unlike H-Ap and B-Ap which undergo rapid substitutions, the crystal structure of geological Fap was maintained and bands of PO_4^{3-} ions did not change with temperature [51].

In their study, El Gharbi et al. [52] observed by means of XRD patterns that carbonate-fluorapatite of Tunisian phosphate ore changed into fluorapatite when temperature exceeded 900 °C. Knubovets et al. [53] confirmed by FTIR that the peaks of carbonate ions (CO_3^{2-}) substituting (PO_4^{3-}) in francolite decreased with temperature above 870 °C suggesting eventual structural changes into fluorapatite. MattHews et al. [54] suggested that carbonate fluorapatite was decomposed into fluorapatite between 599 and 747 °C (Equation 4). However, the substitution of carbonate ions (CO_3^{2-}) in fluorapatite may be the reason behind the lower stability of carbonate fluorapatite compared to fluorapatite [55].

$$Ca_{5-1/2x}[(PO_4)_{3-x}(CO_3)_x](F,OH) \rightarrow Ca_5(PO_4)(F,OH) + CaO + CO_2 \quad (4)$$

2.3.2 Kinetic analysis of thermal decomposition of phosphate ore

The objective of this section is to discuss critically the state of the art of kinetic modeling in the thermal decomposition of phosphates ore. Furthermore, this section will throw light on characteristics of other relevant multistep processes that are not yet considered in thermal decomposition of phosphates literature to improve the reliability of kinetic data.

The kinetics of thermal decomposition of phosphate ore has been studied by two approaches: the isothermal approach and the non-isothermal approach. The isothermal method describes the overall rate of carbon dioxide gas production from phosphate ore using a tubular furnace or TGA handling

a significant amount of sample that can be characterized. The non-isothermal approach provides the global apparent activation energy of the overall process as the sum of the reaction rate of different volatilization reactions. Non-isothermal experiments are performed on TGA. This equipment is equipped with thermobalances to monitor the instantaneous change of mass loss of the sample according to the temperature or time. The primary limitation of TGA is that previous studies assumed that the overall rate of mass loss can be represented by a single step, which results in inaccurate kinetic data. Except for one study, which split the mass loss curves into individual steps according to the thermal behaviour of the ore. Both approaches have ensured a good agreement between experimental data and reaction models despite the difference in setup configuration and effect of procedural parameters affecting the reliability of kinetics data. However, it is not rational to compare the kinetic results of various studies to investigate the intrinsicality of kinetics parameters because of the dissimilarity of operational conditions (heating rate temperature program) and reactants (reactivity, composition, and distribution of phases, particle size). Hence, it is not rational to compare the kinetic results of various studies to investigate the intrinsicality of kinetics parameters. Furthermore, there is an inconsistency in determining the conversion since some researchers used the mass loss of the entire sample (TGA-non-isothermal experiments). Some researchers characterized the treated product or analyse the evolved gas with analytical techniques to calculate carbon release (Furnace and TGA coupled with FTIR). More details are provided in the subsequent sections.

Banane et al. [56] studied the kinetics of thermal decomposition of phosphate ore (200-315 µm) originated from Iraq with a high concentration of carbonate minerals, using TGA between 25 and 1000 °C for single heating of 1.374 °C/min. They first characterized the rocks with XRD, which

suggested that Iraqui phosphate ores contain 16 % of carbonate minerals. The phosphorus-bearing mineral in both rocks was fluorapatite ($Ca_{10}(PO_4)_6F_2$). The non-isothermal Freeman Carroll method (Equation 5) assuming n-order reaction models, demonstrated that the global process obeys to 0 order reaction model with an activation energy of 45 Kcal/min and pre-exponential factor of $8.8x10^{-6}$ s^{-1}. Although the authors recognized that the process occurs in three main steps without specifying the transformation in each step, they applied a global kinetic model. Hence, adoption of global kinetics models may result in meaningless kinetic data because it does not allow the determination of mechanisms describing each step. This approach can provide inaccurate kinetic results, especially when magnitudes of kinetics parameters of individual steps are significantly different. Moreover, Freeman Carroll method has many limitations that can limit its application in global kinetic modeling: i) sensitivity of reaction order toward the number of points to fit ii) non-direct determination of pre-exponential factor iii) limited to n-order reactions [57]. Furthermore, the method is differential, and further efforts are required to calculate the rate of reaction term, especially when dealing with traditional TGAs which do not display DTG curves. Differentiation of TG data can result in noisy data.

$$\frac{-(E/R)\Delta(1/T)}{\Delta ln(1-X)} = \frac{\Delta ln(dX/dt)}{\Delta ln(1-X)} - n \qquad (5)$$

Where, E is the activation energy (KJ/mole), X conversion calculated from mass loss, n is reaction order.

Bilali et al. [58] performed a kinetic analysis of phosphate ore pyrolysis (150 cm3/min N2) with the famous non-isothermal Coats-Redfern method using tubular reaction at four heating rates 1.7, 10, and 21 °C/min in the temperature range RT-900 °C. The main impurities of the apatitic

phosphate ore are calcite, dolomite, and organic matter. The rock is also rich in oil and aromatic compounds. The researchers applied gas chromatography-mass spectroscopy and nuclear magnetic resonance to analyze the gases and oil produced from the pyrolysis, respectively. Three main steps were suggested: 1) removal of moisture at 25-100 °C, 2) decomposition of kerogen to bitumen at 200-500 °C, and 3) calcination of calcite and dolomite at 600-900 °C. The authors reported that pyrolysis has a pathway of two consecutive reactions. The non-linearity of the left-side of the Coats-Redfern equation (Equation 6) versus 1/T, giving two discontinuous straight lines, implies the occurrence of two successive reactions. The first step is the breaking of weak chemical bonds of kerogen, which dissociates into bitumen. They did not assign the second reaction, which must correspond to the calcination of carbonate minerals. The authors concluded that the kinetics parameters of both steps depend on the heating rate. The kinetics parameters of pyrolysis for each heating rate are summarized in Table 2-2.

Activation energy and pre-exponential factor are invariant parameters, but they are affected by heating rate as a procedural parameter. One cannot distinguish between DTG curves corresponding to each heating rate. However, it is very known that the peak temperature of DTG increases strongly with the heating rate [59] due to the significant temperature gradient between the sample and furnace. Such phenomena should be attributed to the thermal lag that becomes significant at high heating rates [60, 61]. Moreover, if one uses the non-isothermal equation Coats-Redfern or differential method for non-isothermal conditions to estimate kinetic parameters, he will notice that the rate of reaction $d\alpha/dt$ (i.e. activation energy and pr-exponential factor) is governed by the heating rate. The compensation effect approach is a method to testify how activation energy and pre-exponential factor relationship is affected by heating rate [62].

$$ln\frac{g(X)}{T^2} = ln\left[\frac{AR}{\beta E_a}\left(1-\frac{2RT}{E_a}\right)\right] - \frac{E_a}{RT} \quad (6)$$

Where, X is the conversion of reaction, A is pre-exponential factor, β is heating rate, Ea is activation energy, R is gas constant, f(X) and g(X) are differential and integral reaction model, respectively.

Naktiyok et al. [63] combined isoconversional methods and model fitting to perform kinetics analysis of aliphatic phosphate ore rich in organic matter using TGA under nitrogen gas at four heating rates 2.5, 5, 10 and 20 °C/min between 298-873 K. The trend of DTG curves confirmed also that the process consists of two steps: 1) removal of moisture and volatile compounds between 383 and 523 K depending on temperature 2) decomposition of organic matter including hydrocarbons and volatilized oil at 533 and 873 K depending on the heating rate. The isoconversional methods Kissinger–Akahira–Sunose (KAS) and Flynn–Wall–Ozawa (FWO) suggested that the thermal decomposition is complex involving two main steps that require independent analysis. Nevertheless, both methods provide similar activation energy for each step (1st step: $E_{KAS,a}$=62.43 KJ/mole, $E_{FWO,a}$=65.87 KJ/mole / 2nd step: $E_{KAS,a}$=120.44 KJ/mole, $E_{FWO,a}$=124.16 KJ/mole). Analysis with model fitting methods using the Ortega method demonstrated that the first step is controlled by 2D diffusion while the rate-limiting step of the second step is 3D diffusion. Hence, this shift of reaction mechanism is important, indicating the complexity of the process. It is worth nothing that the tested phosphate ore does not contain calcite nor dolomite. However, the FWO and KAS are derived from mathematical approximations such as Doyle's approximation because temperature integral does not have any analytical solution [64]. Such approximations may lead to inaccurate kinetic data [65]. These mathematical approaches are simplified solutions of integral temperature equation that does not have an analytical solution. Hence, using these integral methods may lead to a misestimate of activation energy. To address

these limitations, many more reliable isoconversional methods such as the Friedman and Vyazovkin developed without setting any assumptions or hypotheses that can be applied [67]. Friedman method is a different approach that can give more accurate activation energy as it does not require any simplification. However, differentiation of mass loss to obtain rates may create noise when TGA does not provide DTG curves. Such numerical differentiation may result in inaccurate kinetic data.

Aouad et al. [66] compared kinetic parameters of thermal decomposition natural phosphate ore containing 4% of kerogen, decarbonated phosphate, and then synthetic kerogen extracted from phosphate ore matrix. The study aimed was to investigate the effect of the presence of organic matter and kerogen on the kinetic behaviour of natural phosphate ore. The experiments were conducted on TGA under a nitrogen atmosphere at the temperature RT-1200 °C. The results showed that at a fixed heating rate of 5 °C/min, the activation energy of thermal decomposition of natural was the highest, followed by decarbonated phosphate ore and then synthetic kerogen. Such results indicate that the removal of organic matter from phosphate ore requires high temperatures, which drive the process to shift toward higher temperatures. Kinetics parameters for various samples at different heating rates are summarized in Table 2-2.

Olson [67] studied kinetics of phosphate ore pyrolysis combining rotary kiln and TGA. The isothermal experiments performed at 200-1000 °C data were fitted to 0^{th},1^{st} , and 2^{nd} order reaction models. Configuration of rotary kiln restricted the author to perform his kinetic analysis under isothermal conditions. Preliminary experiments were conducted to determine the temperature profile inside the rotary kiln and locate isothermal zones. The second set of experiments was carried out on the TGA mimicking the temperature profile of the rotary kiln, which has non-uniform

temperature distribution. These experiments aim to provide the kinetic parameters of the overall process of phosphate ore pyrolysis and the kinetic behaviour of its major constituents that include carbonates, water, and ultimate analysis elements (C, H, N, O, S) using LECO. C, H, O, and S were incorporated into both minerals and organic matter, and N was incorporated into the organic matter only. The kinetics of devolatilization of carbonate, vaporization of water, and ultimate analysis elements volatilization were conducted by analyzing the residual product. The kinetics of the overall devolatilization was studied by monitoring mass loss. The results showed that reaction order shifts according to residence time at each temperature. This reaction order shifted to avoid the mismatch between experimental data and predicted data. It is noteworthy that Olson [67] included a constant time in the proposed mathematical model. It is related to the time required to reach the desired temperature during heating-up. Hence, adopting the isothermal program and performing experiments at high temperatures may also be a source for deviations. In this regard, Vyazovkin and Wight [68] reported that when the reaction proceeds before reaching the desired temperature, the reaction can progress, leading to inaccurate kinetic data. It is possible to use high heating rates to address this problem. However, this results in a poor heat transfer with a non-uniform temperature of the sample. Kinetics parameters calculated by Olson are summarized in the Table 2-2.

Table 2-2 Different kinetic models for the thermal decomposition of phosphate ore

Composition of phosphate ore	Reactor	Temperature Program	Particle size	Steps	Method of kinetic analysis	Activation energy	Pre-exponential factor	Ref.
$Ca_{10}(PO_4)_6F_2$, Carbonate minerals: 16% organic matter	TGA	RT-1000 °C (1.374 °C /min)	200-315 µm	Dehydration : 20-200 °C Removal of organic matter: 200-550 °C Decomposition of carbonate: 600-850 °C	Zero order reaction model (carroll-freeman method)	Ea(500-870 °C) = 45 Kcal/mole	$A=8.8x10^{-6}$ s^{-1}	[56]
$Ca_{10}(PO_4)_6F_2$:90%, $CaCO_3$:2.6% $Ca_3Mg(CO_3)_2$:1.8% Clays:1.2% SiO2:1.4% Organic matter: 2.8%	TGA (150 cm3/min N2)	RT-900 °C (1.7, 10, and 21 °C/min)	< 1 mm	Removal of moisture at 25-100 °C Decomposition of kerogen to bitumen at 200-500 °C Calcination of calcite and dolomite at 600-900 °C.	First order reaction model (Coats-Redfern equation)	1) Decomposition of kerogen: Ea(1.7 °C/min) = 70.80 KJ/mole Ea(10 °C/min) = 46.22 KJ/mole Ea(21 °C/min) = 46.22 KJ/mole 2) Decomposition of calcite and dolomite: Ea(1.7 °C/min) = 184.7 KJ/mole Ea(10 °C/min) = 81.65 KJ/mole Ea(21 °C/min) = 163.28 KJ/mole	1) Decomposition of kerogen: $A(1.7\ °C/min) = 4.36x10^{4}$ s^{-1} $A(10\ °C/min)=1.4x10^{5}$ s^{-1} $A(21\ °C/min) = 3.6x10^{11}$ s^{-1} 2) Decomposition of calcite and dolomite: $A(1.7\ °C/min) = 1.2x10^{4}$ s^{-1} $A(10\ °C/min)=3.49x10^{5}$ s^{-1} $A(21\ °C/min) = 6.22x10^{11}$ s^{-1}	[58]
Aliphatic phosphate ore	TGA(nitrogen gas)	298-873 K (2.5, 5, 10 and 20 °C/min)	< 100 µm	Removal of moisture and volatile compounds between 383 and 523 K depending on heating rate. Decomposition of organic matter including hydrocarbons and volatilized oil at 533 and 873 K depending on the heating rate.	KAS, FWO, model fitting method with solid-state reactions	1st step: Isoconversional methods: $E_{KAS,a,mean}$=62.43KJ/mole $E_{KAS,a,mean}$=65.87 KJ/mole 2D diffusion: 62.83-73.4 KJ/mole (depending on heating rate) 2nd step: Isoconversional methods: $E_{KAS,a,mean}$=120.44KJ /mole $E_{KAS,a,mean}$=124.16KJ /mole 3D diffusion: 117.27-141.21 KJ/mole (depending on heating rate)	N/A	[63]

Apatite: 86.6% Silicates: 7.9% Kerogen: 4.8% Bitumen: 0.4%	TGA	RT-1200 °C (5, 20, 50, 100 °C/min)	N/A	N/A	First order reaction model (Coats-Redfern equation)	Ea(5 °C/min) = 50.41 KJ/mole Ea(20 °C/min) = 47.44 KJ/mole Ea(50 °C/min) = 53.50 KJ/mole Ea(50 °C/min) = 71.63 KJ/mole	A(5 °C/min) = $2.13x10^6$ s^{-1} A(20 °C/min)=$19.68x10^6$ s^{-1} A(50 °C/min) = $25.67x10^6$ s^{-1} A(100 °C/min) = $4.68x10^6$ s^{-1}	[66]
Decarbonized phosphate	TGA	RT-1200 °C (5°C/min)	N/A	N/A	First order reaction model (Coats-Redfern equation)	Ea = 47.38 KJ/mole	A = $2.83x10^6$ s^{-1}	[66]
N/A	TGA	200-1000 °C (143°C/min)	N/A	2.95 mm	0^{th},1^{st} , 2^{nd} reaction model	Individual processes: Volatilization C:10.994kcal/mole Volatilization H:15.907kcal/mole Volatilization O:5.734kcal/mole Water removal:1.277kcal/mole	Individual processes: Volatilization C: $7.479x10^{12}$ s^{-1} Volatilization H:4.052 $x10^{14}$ s^{-1} Volatilization O:5.2.598 $x10^{11}$ s^{-1} Water removal: 0.004 s^{-1}	[67]

CHAPTER 3 MATERIALS AND EXPERIMENTAL TECHNIQUES

3.1 Material preparation

The low-grade phosphate ore used in this study was provided by Office Chérifien des Phosphates (OCP) Morocco with moderate particle size (~4cm). The large samples (1 Kg) of phosphate ore were reduced into smaller representative sizes according to ASTM C702 to maintain similar characteristics. Firstly, the phosphate ore was mixed thoroughly by turning the large sample to ensure a good homogenization. A conical pile with uniform height and diameter was then formed. The 1 Kg of sample cone was then divided into four equal quarters. Two diagonally opposite quarters were removed while the remaining two diagonally opposite quarters were mixed for further coning until reaching the desired size of phosphate ore (50 gram).

Each 50 grams of phosphate ore was crushed, ground, and then sieved into µm 53-106 µm using a sieve shaker to ensure a good agitation and separation of particles. This size distribution was assumed to be above the fine particle that can undergo agglomeration during the process. The riffle splitter, which split the material into two equal fractions, was employed to reduce the size of sieved phosphate ore to ensure a good homogenization.

3.2 Characterization

3.2.1 Inductively coupled plasma optical emission spectroscopy (phosphate ore)

Inductively coupled plasma optical emission spectroscopy (ICP-OES) is a commonly used technique in material characterization. The plasma is the energy generated from an ionization source to excite the components elements (atoms). The electrons absorbing this energy become

excited, reaching a higher energy level. The excited atoms then release that energy as spectrum rays (photons) with different wavelengths to achieve the lowest energy level (ground level energy) for their stability. The presence of an element type is validated based on the position of the spectrum rays measured by the spectrometer. The intensity determines the concentration of the detected element.

The obtained samples with 53-106 µm were analyzed by the high-temperature digestion method. 1 g of phosphate ore samples was weighed and mixed with 1 g of the appropriate fusion mixture (lithium borate flux). The mixture was poured into a platinum crucible and then subjected to a high temperature of 1200 °C and vigorous agitation in a heating chamber of a Fusion fluxer for 15 minutes. The fusion mixture melts, forming a eutectic mixture that digests phosphate ore to form a heterogeneous liquid. After the fusion process, the molten mixture is poured into a platinum mold and then filled in a tube with the addition of distilled water until reaching 100 ml.

The digested samples were then sent to Agilent 5100 SVDV ICP-OES for elemental analysis that requires liquid samples for significant accurate analysis. Elemental composition of low-grade phosphate ore is summarized in Table 3-1. This data was used to determine mineralogical composition with XRD.

Element	Concentration (%)
P (%)	10.5
Ca (%)	31.7
Mg (%)	0.8
Si (%)	-
Fe (%)	0.1
Cu(ppm)	172.3
Zn (ppm)	22.1
Cr (ppm)	12.8
Cd (ppm)	20.2

Table 3-1 Elemental composition of low-grade phosphate ore with ICP-OES

3.2.2 X-Ray Diffraction (XRD)

X-Ray Diffraction (XRD) is an analytical technique used to identify the crystals present in a material. An X-ray source bombards the analyzed material to detect the crystals. XRD peaks are produced at specific angles (2θ) that represent the fingerprint of periodic atomic arrangements of crystals. Powder XRD Analyses were carried out with a Philips X'PERT X-ray diffractometer. The diffractometer is equipped with a Cobalt X-rays source and of X-rays and two X-ray detectors. The 2θ angle was ranged between 5º and 80º to collect the patterns of crystals. The produced XRD

patterns were collected and compared to the Inorganic Crystal Structure Database (ICSD) to identify the crystals.

It is worth noting that the XRD detector can not generally identify phases with less than 5%. XRD was used to track the behaviour of crystalline phases during thermal decarbonization of phosphate ore.

3.2.3 LECO

LECO is an analytical method used to measure the concentration of carbon and sulfur in metallic samples. The LECO technique is based on the principle of combusting the sample at high temperatures 1000 ºC in an induction setup under oxidizing atmosphere converting the carbon and sulfur into their oxidizing products: carbon dioxide and sulfur dioxide. The escaping gases pass through an infrared detector and give a signal proportional to the concentration. LECO technique was used to determine the concentration of carbon during thermal decarbonization of phosphate ore. This technique enabled the validation of the data provided by XRD to understand the transformation of carbon-bearing minerals during thermal decarbonization of phosphate ore. Phosphate ore was dried in a furnace at 150 ºC for 24 hours to remove humidity before chemical analysis with LECO.

3.3 Thermodynamic analysis

The thermal decarbonization of the phosphate ore process was simulated employing the Equilib model of Factsage^{TM} software to predict the chemical species and corresponding concentrations when the system reaches the equilibrium state of the system [69]. The equilibrium data is calculated using the well-known Gibbs free energy minimization method, which predicts at constant pressure and temperature the progress of complex systems that involve multi-component

and multi-phase systems without the need for knowledge of exact stoichiometric equations of multi- reaction system [70-72]. The thermodynamic simulation enabled us to reveal the influence of temperature on the decarbonization of carbon-bearing minerals. The databases selected to simulate a carbothermal reduction of phosphate ore were FactPS (pure substances) and FToxid (Stoichiometric metal oxides). Equilib model was used to provide a good understanding of interactions between different minerals during thermal decarbonization of phosphate ore regardless of the kinetic behaviour of the system and degree of association between minerals in the phosphate ore matrix.

3.4 Experimental setups

3.4.1 Electric furnace

A series of experiments were carried out on a muffle furnace under air to investigate the phase transformation during thermal decarbonization of phosphate ore. The furnace was heated up to setpoint temperature 700-900 °C. Experiments were performed in the temperature ranging between 700 and 900 °C with an increment of 100 °C (Table 3-2). The alumina crucible was filled with 2 grams of phosphate ore and then placed in the center to exhibit uniform thermal heating at the setpoint temperature and kept for 10-70 min. The decarbonized phosphate was then analyzed by XRD to identify the phases at each temperature and residence time of 40 min. The residence time 40 min was selected for characterization because it is the longest duration at 800 °C to achieve maximum mass loss in the furnace.

Table 3-2 Operational conditions of thermal decarbonization using muffle furnace

Atmosphere	Air
Particle size	53-106 µm
Isotherms	700-900 ºC with a step of 100 ºC
Residence time	10-70 min with a step of 10 min

3.4.2 Thermogravimetry analysis

3.4.2.1 Setup

Thermogravimetry analysis (TGA) is a technique to investigate the thermal stability of materials by recording the change of mass caused by gas formation as a function of time or temperature. Thermogravimetric analyzers are equipped with electronic thermobalances to measure the instantaneous mass of the sample. The mass loss is attributed to chemical or physical phenomena such as decomposition, evaporation, and dehydration.

Preliminary experiments were conducted to determine the optimum sample size of mixture phosphate ore that reduces the heat transfer resistance due to thermal conductivity of chemical species and minimize the difference between the reference temperature and actual temperature of the analyzed sample. It is worth noting that thermocouples of modern TGAs measure temperature outside the mixture. The sample size of powders was around 15 mg poured into a platinum pane (100 µL) and then subjected to heat up to 1000 °C at four heating rates 2, 4, 8, and 20 °C/min (Table 3-3). Slow heating rates were selected for better visualization of steps and for reducing thermal lag. The platinum pane was selected to hinder any possible interaction between the pane and sample that can alter the accuracy of kinetic results and the actual thermal behaviour. For each material, the sample size was decreased gradually until observing non-mass dependence of TG

curves. The experiments were conducted using the thermogravimetric analyzer Q 550 of TA instruments (Figure 3-2).

Table 3-3 Operational conditions of thermal decarbonization using TGA

Particle size	53-106 µm
Temperature range	From room temperature to 1000 °C
Heating rate	2, 4, 8, and 20 °C/min

The objective of the TGA experiments was to perform the kinetic analysis of the thermal decarbonization of phosphate ore between room temperature and 1000 °C under nitrogen gas atmosphere by combining isoconversional methods and model fitting methods. Gas nitrogen was used instead of air due to technical restrictions of setup. However, it was assumed that the environment (air or nitrogen) does not affect the nature of stable phases.

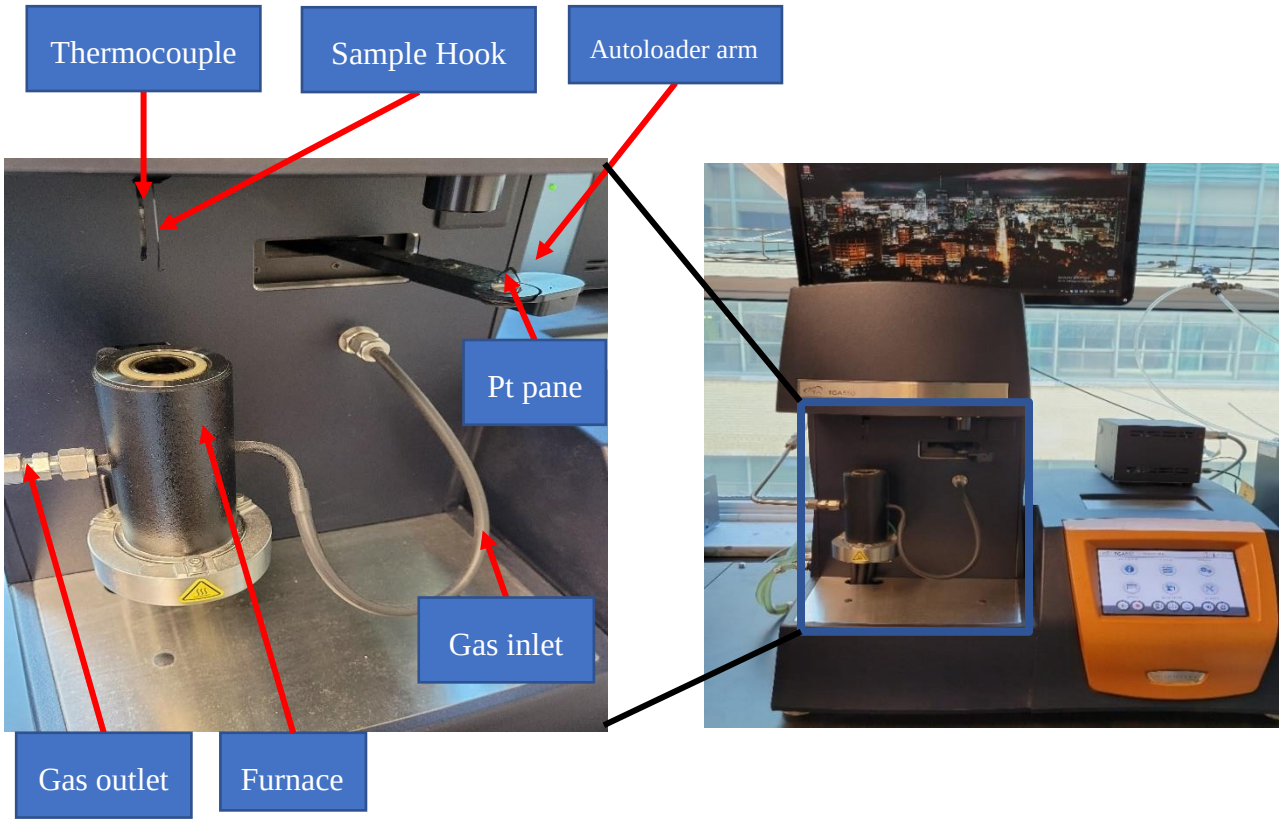

3.4.2.2 Kinetic modeling

To perform kinetic analysis of thermal decarbonization of phosphate ore, we applied two common techniques: isoconversional methods and model-fitting methods that are widely used in thermal analysis [64].

The rate of solid-state reactions is represented by:

$$\frac{d\boldsymbol{\alpha}}{dt} = k(T)f(\boldsymbol{\alpha}) \quad (8)$$

Where $k(T) = Ae^{-\frac{E_a}{RT}}$ in which K(T) is the reaction constant (s^{-1}), A is the pre-exponential factor (s^{-1}), R is the universal gas constant ($J \cdot K^{-1} \cdot mol^{-1}$) and Ea is the activation energy ($J \cdot mole^{-1}$), f(α) is the reaction model and α is the degree of conversion. It is calculated from the mass loss data obtained from TGA (Equation 9).

$$\alpha = \frac{m_i - m_t}{m_i - m_f} \quad (9)$$

Where m_i, m_t and m_f are the initial sample mass, the sample mass at given time t and the final sample mass, respectively.

3.4.2.3 Isoconversional methods

Isoconversional methods assume that reaction rate depends only on temperature and conversion, and kinetics parameters do not depend on the heating rate. Isoconversional methods (free-model methods) are commonly used in the thermal analysis because of their advantages. These techniques allow the estimation of activation energy without requiring the determination of the reaction model. They are also helpful for details of complex chemical processes that include more than one

step (decomposition of heterogenous materials) [64]. Nevertheless, the isoconversional methods are limited only to single-step processes in which the apparent activation energy is assumed constant. Kinetics theory states that the Arrhenius equation is applied only for one-step reactions. Hence, activation energy and pre-exponential factor should be unchanged, and any significant change of activation energy versus the conversion implies that the process is complex involving a combination of multistep reactions (parallel, successive) [64, 68, 73, 74].

According to the recommendations of Vyazovkin et al. [64], four heating rates were applied to conduct isoconversional methods, and activation energy as a function of the degree of conversion α was calculated between 0.2 and 0.9 with a step of 0.1. The apparent activation energy was calculated from four isoconversional methods that include methods such as Ozawa, Flynn, and Wall (OFW), Kissinger-Akahir Sunose (KAS), Starink, and Vyazovkin.

❖ Ozawa, Flynn and Wall (OFW)

OFW method is resulted from Doyle approximation of the temperature integral that does not have any analytical solution [64]. The obtained equation (Equation 10) in OFW method represents a linear relationship between ln(β_i) and $T_{\alpha,i}$. The plot of ln(β_i) versus $1/T_{\alpha,i}$must yield straight line for each selected degree of conversion α. Then, the activation energy $E_{a.\alpha}$ is calculated from the slope.

$$ln(\beta_i) = C_{OFW} - 1.052\frac{E_{a.\alpha}}{RT_{\alpha,i}} \quad (10)$$

❖ Kissinger-Akahira and Sunose (KAS)

The KAS method is more accurate than OFW method to estimate the apparent activation energy [64]. In Equation 11, $ln\left(\frac{\beta_i}{T_{\alpha,i}^2}\right)$ is plotted versus $1/T_{\alpha,i}$ to give a straight line for each value of α to calculate the activation energy.

$$ln\left(\frac{\beta_i}{T_{\alpha,i}^2}\right) = C_{KAS} - \frac{E_{a.\alpha}}{RT_{\alpha,i}} \tag{11}$$

❖ Starink

In Starink equation, $ln\left(\frac{\beta_i}{T_{\alpha,i}^{1.92}}\right)$ is plotted versus $1/T_{\alpha,i}$ to give a straight line for each value of α to calculate the activation energy (Equation 12).

$$ln\left(\frac{\beta_i}{T_{\alpha,i}^{1.92}}\right) = C_{ST} - 1.008\frac{E_{a.\alpha}}{RT_{\alpha,i}} \tag{12}$$

❖ Vyazovkin

Vyazovkin method is derived from the assumptions that reaction model is independent on heating rate [75]. The method is developed without setting any approximation of integral temperature. Activation energy is estimated by minimizing the right side of Equation 13 in which $\phi(Ea)$ is the objective function.

$$\phi(Ea) = Min\sum_{i}^{n}\sum_{j\neq i}^{n}\frac{I(E_{\alpha,}T_{\alpha,i})\beta_j}{I(E_{\alpha,}T_{\alpha,j})\beta_i} \tag{13}$$

Where $\phi(Ea)$ is the function of integral isoconversional method, $I(E_{\alpha,}T_{\alpha,i})$ is integral temperature, i and j denote the script of heating rates β_i and β_j.

$I(E_{\alpha,}T_{\alpha,i})$ is expressed as follow:

$$I(E_{\alpha,}T_{\alpha,i}) = \frac{E_\alpha}{R}p(x) \quad (14)$$

Where x=E/RT. Farjas and Roura [65] proposed an accurate analytical approximation (Equation 15) of p(x) for x>12 to solve Vyazovkin model.

$$p(x) = \frac{exp(-x)}{x}\frac{x^5 + 40x^4 + 552x^3 + 3168x^2 + 7092x + 4320}{x^6 + 42x^5 + 630x^4 + 4200x^3 + 12600x^2 + 15120x + 5040} \quad (15)$$

3.4.2.4 Model fitting methods

Model fitting methods are employed to determine the dependence of the reaction rate on the conversion of heterogeneous chemical processes throughout a mechanistic reaction model of the rate-limiting step. These methods are frequently coupled with isoconversional models to yield accurate kinetic data for solid-state reactions. The apparent activation energy calculated from isoconversional methods is commonly used as an initial guess value for fitting experimental data with kinetic models.

Coats-Redfern is one of the most popular model-fitting methods, and it is used exclusively for non-isothermal conditions to perform kinetic analysis. This method is widely in solid-state reaction processes because it simultaneously determines kinetic triple (reaction model, activation energy, pre-exponential). The Coats-Redfern, which is given by Equation 16, was employed in this research to determine the most representative mechanism that controls the decomposition and to estimate the corresponding kinetic parameters. Although the model-fitting methods require a single heating rate to estimate kinetics parameters, we studied the effect of heating rate on these parameters. Table 3-4 shows the most suitable models that can describe the decomposition of

minerals. We limited the number of solid-state reaction models based on the fundamentals of thermal decomposition of minerals and characteristics of low-grade phosphate ore.

$$ln\frac{g(\alpha)}{T^2} = ln\left[\frac{AR}{\beta E_a}\left(1-\frac{2RT}{E_a}\right)\right] - \frac{E_a}{RT} \quad (16)$$

Where g(α) is the integral kinetic model function of mechanisms, α is the degree of conversion, β is heating rate, R is the universal gas constant, E_a is the activation energy and A is the pre-exponential factor.

The kinetic parameters are obtained by plotting $\ln\frac{g(\alpha)}{T^2}$ versus $\frac{1}{T}$, in which activation energy is calculated from the slope of a straight line. The intercept of the straight line with the Y-axis $\left(\ln\frac{g(\alpha)}{T^2}\right)$ gives the pre-exponential factor. Fitting experimental data with proposed models was performed by evaluating the residual sum of squares (RSS) (Equation 17) and the correlation coefficient (R2) of the left-hand side of experimental data $\ln\frac{g(\alpha)}{T^2}$ versus $\frac{1}{T}$. The $\left(ln\frac{g(\alpha)}{T^2}\right)_{exp}$ was calculated from the degree of conversion and corresponding temperature for linear heating rate. β, T, R, and the predicted values of E, A of the right-hand side of the Coats-Redfern equation (Equation 16) substituted $\left(ln\frac{g(\alpha)}{T^2}\right)_{calc}$. The best reaction model is the one that has the minimum value of RSS and the maximum value of R^2. Advanced optimization tools were employed to find the global minimum to give accurate kinetic parameters.

A code was written in Matlab language to solve Coats-Redfern equation to estimate the kinetic parameters. Advanced optimization tools were employed to find the local minimum.

$$RSS = Min\sum(\left(ln\frac{g(\alpha)}{T^2}\right)exp - \left(ln\frac{g(\alpha)}{T^2}\right)calc)^2 \quad (17)$$

Table 3-4 Kinetic models of mechanisms of solid-state [76]

Model	g(α)	**f**(α)
	Geometrical contraction	
Contraction area (R2)	$1-(1-\alpha)^{1/2}$	$2(1-\alpha)^{1/2}$
Contraction area (R3)	$1-(1-\alpha)^{1/3}$	$3(1-\alpha)^{2/3}$
	Nucleation	
Avrami-Erofeyev (A2)	$[-ln(1-\alpha)]^{1/2}$	$2(1-\alpha)[-ln(1-\alpha)]^{1/2}$
Avrami-Erofeyev (A3)	$[-ln(1-\alpha)]^{1/3}$	$3(1-\alpha)[-ln(1-\alpha)]^{2/3}$
	Diffusion	
1-D diffusion (D1)	α^2	$\frac{1}{2\alpha}$
2-D diffusion (D2)	$(1-\alpha)ln(1-\alpha)+\alpha$	$\left[\frac{-1}{ln(1-\alpha)}\right]$
	Reaction-order	

1st order reaction (F1)	$-ln(1-\alpha)$	$(1-\alpha)$
2nd order reaction (F2)	$\frac{1}{1-\alpha}-1$	$(1-\alpha)^2$

CHAPTER 4 PHASE TRANSFORMATION DURING LOW-GRADE PHOSPHATE ORE DECARBONIZATION

4.1 Phase transformation with XRD analysis

The main minerals of low-grade phosphate ore detected by XRD are carbonate fluorapatite ($Ca_{9.55}(PO_4)_{4.96}F_{1.96}(CO_3)_{1.283}$), calcite ($CaCO_3$), dolomite ($CaMg(CO_3)_2$), and quartz ($SiO_2$) (Table 4-1). Carbonate-fluorapatite formula was obtained from XRD analysis. The content of different minerals is mentioned in Table 4-1. Carbonate fluorapatite occurs as a result of partial substitution of both orthophosphate group (PO_4^{3-}) and fluoride ions (F^-) of fluorapatite ($Ca_{10}(PO_4)_6F_2$) structure by carbonate ions (CO_3^{2-}) as impurities. Carbonate fluorapatite was also found as a phosphorus-bearing mineral in other phosphate deposits [77, 78].

Table 4-1 Mineralogy of low-grade phosphate ore with XRD

Mineral	Content (%)
$Ca_{9.55}(PO_4)_{4.96}F_{1.96}(CO_3)_{1.283}$	48.8
SiO_2	16.9
$CaMg(CO_3)_2$	26.1
$CaCO_3$	8.2

Some clarification and hypotheses were considered before discussing crystalline phase transformation during thermal decarbonization of low-grade phosphate ore with XRD. Figure 4-1 shows that carbonate fluorapatite ($Ca_{9.55}(PO_4)_{4.96}F_{1.96}(CO_3)_{1.283}$) and fluorapatite ($Ca_{10}(PO_4)_6F_2$) have close XRD patterns (2θ, intensity).

These features imply that the incorporated carbonate ions in the fluorapatite structure do not strongly affect the diffraction patterns. The similarity of peaks makes distinguishing between $Ca_{9.55}(PO_4)_{4.96}F_{1.96}(CO_3)_{1.283}$ and $Ca_{10}(PO_4)_6F_2$ quite challenging and thus does not help to accurately verify if $Ca_{9.55}(PO_4)_{4.96}F_{1.96}(CO_3)_{1.283}$ is converted to $Ca_{10}(PO_4)_6F_2$ and determine the corresponding temperature of this transformation. LECO was used to solve this problem based on the mass balance of carbon. The first information is that XRD showed that low-grade phosphate ore contains 48.8% of $Ca_{9.55}(PO_4)_{4.96}F_{1.96}(CO_3)_{1.283}$, 26.1% of $CaMg(CO_3)_2$, and 8.2% of $CaCO_3$ as the main carbon-bearing minerals (Table 4-1). The second information is that $Ca_{9.55}(PO_4)_{4.96}F_{1.96}(CO_3)_{1.283}$ contains theoretically 12% of carbon, while $CaMg(CO_3)_2$ and $CaCO_3$ have 13.03 and 12.01 % of carbon, respectively. Hence, $Ca_{9.55}(PO_4)_{4.96}F_{1.96}(CO_3)_{1.283}$, $CaMg(CO_3)_2$, and $CaCO_3$ contributed with 57, 33.43, and 9.53 % of carbon in phosphate ore, respectively. This carbon distribution is valid only if phosphate ore does not contain organic matter or another amorphous phase. Moreover, LECO analysis (Figure 4-3) showed that 81.86% of carbon is removed at 800 °C for 40 min. Hence, it was assumed that $Ca_{9.55}(PO_4)_{4.96}F_{1.96}(CO_3)_{1.283}$ is transformed to $Ca_{10}(PO_4)_6F_2$ at 800 °C for 40 min. Therefore, $Ca_{10}(PO_4)_6F_2$ is indexed at 800 °C for 40 min in Figure 4-2, replacing $Ca_{9.55}(PO_4)_{4.96}F_{1.96}(CO_3)_{1.283}$, although the transformation was not complete as suggested by LECO.

Another observation is that some peaks are shared by more than one crystalline phase because of the complexity of low-grade phosphate and the interesting distribution of minerals.

Figure 4-2 shows crystalline phases present at different stages of thermal decarbonization of low-grade phosphate ore (700, 800 and 900 °C for 40 min). The peaks collected for ore at 30.81º, 52.16º, 59.68º ascribed to $CaMg(CO_3)_2$ disappeared at 700 ºC and 40 min, except the peak at 30.81º whose intensity sharply decreased. It should be noted that peak at 59.68º is shared also by SiO_2.

This trend was compensated by the appearance of new peaks at 37.14º attributed to Mg_2SiO_4 and $CaMgSi_2O_6$ and at 29.40ºand 69.99º ascribed to $CaCO_3$. There is also a significant increase of intensity at 31.95º, 39.39º, and 49.60 º attributed to Mg_2SiO_4 and $CaMgSi_2O_6$ and at 35.62º and 55.20º attributed to Mg_2SiO_4. These changes were accompanied with a slight decrease of intensities at 20.64º, 42.66º, and 59.94º. These transformations suggest that $CaMg(CO_3)_2$ decomposed to $CaCO_3$, CO_2 and MgO which was not detected because it interacted simultaneously with SiO_2 to form Mg_2SiO_4. Interaction between $CaMg(CO_3)_2$ and SiO_2 to form $CaMgSi_2O_6$ and CO_2 is another reaction taking place within 700 ºC and 40 min.

At 800 ºC and 40 min, $Ca_{9.55}(PO_4)_{4.96}F_{1.96}(CO_3)_{1.283}$ was assumed to have transformed to fluorapatite since LECO analysis (Figure 4-3) suggested that 81.86% of carbon was released in the form of CO_2. Hence, XRD patterns during thermal decomposition were assumed to correspond to $Ca_{10}(PO_4)_6F_2$ with traces of $Ca_{9.55}(PO_4)_{4.96}F_{1.96}(CO_3)_{1.283}$ at 800 °C. Peaks at 56.95º and 70.29º purely ascribed to $CaCO_3$ disappeared and intensity of calcite peaks shared with other crystalline phases at 23.04, 29.40º, 39.37º, and 48.27º of $CaCO_3$ strongly fell. On the other side, intensity of peaks at 26.63º, 39.41º attributed to SiO_2 decreased. These changes were compensated by the formation of new crystalline phases including Ca_2SiO_4 (20.82º, 34.18º, 37.50º, 67.84º) and CaO (37.50º and 67.84º). These changes suggest that $CaCO_3$ decomposed into CO_2 and CaO which then reacted readily with SiO_2 to form Ca_2SiO_4. The peaks attributed to $CaMgSi_2O_6$ disappeared without detecting new crystalline phases.

At 900 ºC and 40 min, no new crystalline phase was detected but only more Ca_2SiO_4 and CaO are formed in the expense of SiO_2 and probably $CaCO_3$ that can be formed from decomposition of remaining $Ca_{9.55}(PO_4)_{4.96}F_{1.96}(CO_3)_{1.283}$ as will be discussed later. The sharp increase of peaks intensities at 37.36° and 53.81° corresponding to CaO and Ca_2SiO_4 and decrease of peaks

intensities at 20.92°, 39.25°, and 26.69° corresponding to SiO_2 between 800 and 900 °C confirmed these transformations.

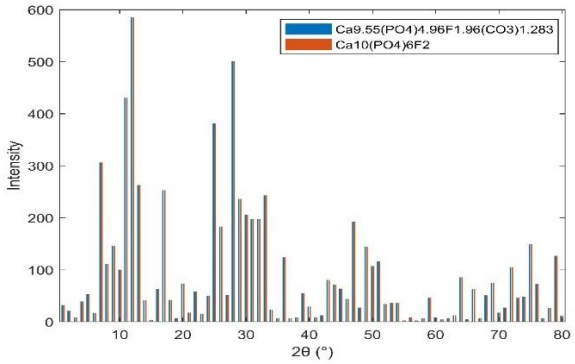

Figure 4-1 Standard XRD patterns of $Ca_{9.55}(PO_4)_{4.96}F_{1.96}(CO_3)_{1.283}$ and $Ca_{10}(PO_4)_6F_2$ from ICSD

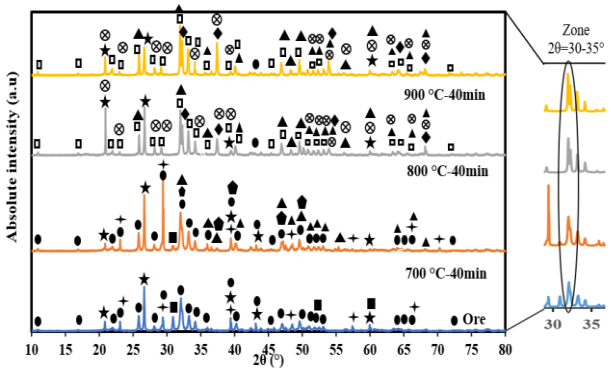

Figure 4-2 XRD patterns during thermal decarbonization of low-grade phosphate ore:

★: SiO_2 - ●: $Ca_{9.55}(PO_4)_{4.96}F_{1.96}(CO_3)_{1.283}$ - ✝: $CaCO_3$ - ■:$CaMg(CO_3)_2$ – ⬟: $CaMgSi_2O_6$- ▲:Mg_2SiO_4- ♦: CaO - ⊗: Ca_2SiO_4 - □: $Ca_{10}(PO_4)_6F_2$

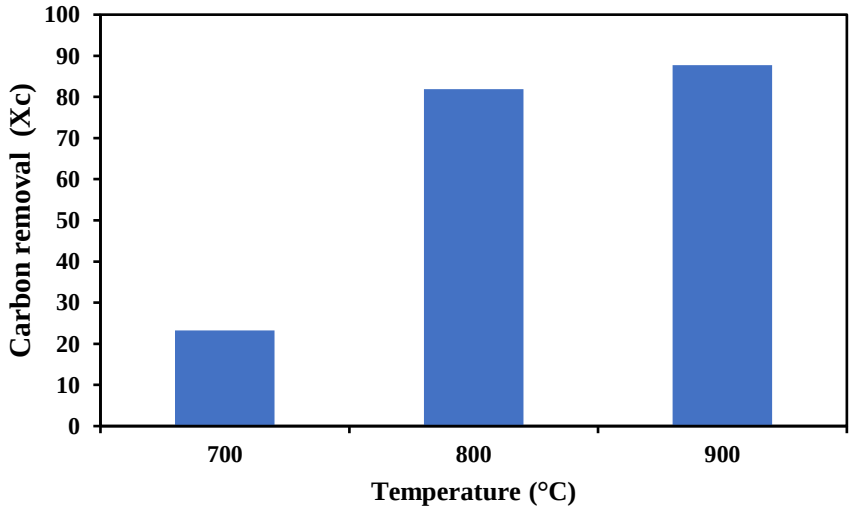

Figure 4-3 Conversion of decarbonization of low-grade phosphate ore at fixed residence time 40 min

4.2 Thermodynamic analysis

4.2.1 Carbonate fluorapatite-Calcite-Dolomite-Quartz system

The equilibrium calculations by Factsage were performed between 25 and 1800 °C at atmospheric pressure using the mineral composition of low-grade phosphate ore (100 kg) provided by XRD (Table 4-1). The objective of these equilibrium calculations was to identify the thermodynamically stable phases and understand the corresponding phase distribution to build a representative reaction pathway of thermal decarbonization of low-grade phosphate ore supported by XRD analysis. The thermochemical properties of $Ca_{9.55}(PO_4)_{4.96}F_{1.96}(CO_3)_{1.283}$ are already integrated in the database of Factsage. The initial minerals forming the low-grade phosphate ore were simultaneously inserted in a single run in Factsage software to run single simulation of the overall composition of low-grade phosphate ore for to take account interactions between them. Among more than 30 major and minor species predicted by the Equilib model, only the major 13 species were considered to investigate crystalline phase distribution and suggest plausible reactions that can occur during the thermal decarbonization process.

Figures 4-4 and 4-5 demonstrate conversion of minerals of low-grade ore as well as evolution of associated products at equilibrium at atmospheric pressure under various temperatures. Equilibrium calculations suggest a complex behavior of thermal decarbonization of low-grade phosphate ore that can be considered as a multistep reactions system with multiple phases and components.

Figures 4-4 and 4-5 show that the amounts of $Ca_{9.55}(PO_4)_{4.96}F_{1.96}(CO_3)_{1.283}$ decreased between 25 and 200 °C. The full disappearance was compensated by the formation of $Ca_{10}(PO_4)_6F_2$, CaF_2, $CaCO_3$, O_2 and CO_2 within the same temperature range. $Ca_{9.55}(PO_4)_{4.96}F_{1.96}(CO_3)_{1.283}$ may decompose to $Ca_{10}(PO_4)_6F_2$, CaO, CaF_2, and CO_2 through two steps. Despite its thermodynamic

feasibility, this transformation was not confirmed experimentally in this temperature interval because XRD and LECO analysis suggested that $Ca_{9.55}(PO_4)_{4.96}F_{1.96}(CO_3)_{1.283}$ begun decomposition between 700 and 800 ºC. The amount of $Ca_{10}(PO_4)_6F_2$ remained unchanged at 200-1000 °C, which implies its high thermal and chemical stability in this complex system. This stability was also proved by XRD analysis.

$CaMg(CO_3)_2$ reacted with SiO_2 at 300 °C to form Mg_2SiO_4 and $CaMgSi_2O_6$ as new stable products. XRD confirmed the formation of these crystalline phases at 700 ºC for 40 min. It is worth noting that Mg_2SiO_4 can also be formed from reaction of SiO_2 and free MgO produced from decomposition of $CaMg(CO_3)_2$. XRD analysis showed that intensities corresponding to SiO_2 does not change significantly, which means that reaction between $CaMg(CO_3)_2$ and SiO_2 is not important. This statement is valid if $CaMg(CO_3)_2$ and SiO_2 are not well associated in phosphate ore matrix. Hence, $CaMgSi_2O_6$ and Mg_2SiO_4 can be formed directly from interaction of SiO_2, CaO and MgO. CaO and MgO are produced from decomposition of dolomite. Hence, calculation of the whole carbonate fluorapatite-Calcite-Dolomite-Quartz system does not completely match with XRD results.

The amount of $CaCO_3$ remained constant until 400 °C and then fell at 500 °C. it was compensated by the formation of $Ca_5Si_2O_7$ and CO_2 at the same temperature. Ca_2SiO_4 was detected by XRD instead of $Ca_5Si_2O_7$. CaO does not appear in Figures 4-4 and 4-5 because it interacts simultaneously with SiO_2 and CaF_2 to form $Ca_5Si_2O_7$ and $Ca_4Si_2F_2O_7$ with a significant increase. The formation of $Ca_5Si_2O_7$ depends on the mass fraction $CaCO_3/(SiO_2/CaCO_3)$. It is worth noting that Ca_2SiO_4 phases can also be formed by SiO_2 and free CaO from decomposition of $CaCO_3$. XRD analysis confirmed only the presence of Ca_2SiO_4 at 800 and 900 °C for 40 min. This implies

that calcium silicate phases are not formed from the interaction between $CaCO_3$ and SiO_2 but only from the interaction between free CaO and SiO_2.

The amount of $CaMgSi_2O_6$ decreased sharply between 500 and 600 ºC. It acted as an intermediate product to form a new stable product $Ca_2MgSi_2O_7$. Reaction between $CaMg(CO_3)_2$ and SiO_2 is feasible above 550 °C for a mass ratio of $CaMg(CO_3)_2$/($CaMg(CO_3)_2$+SiO_2) between 0.6 and 0.8. XRD analysis also confirmed the disappearance of $CaMgSi_2O_6$ at 800 ºC without detection of any new crystalline phase. Lastly, an interaction between CaF_2 and $Ca_5Si_2O_7$ resulted in the formation of $Ca_4Si_2F_2O_7$ at 600 ºC, which was not detected by XRD; this could be attributed to i) poor contact between CaF_2 and $Ca_5Si_2O_7$, ii) the non-formation of $Ca_5Si_2O_7$ as discussed above, and iii) Non-sufficient detection limit of XRD.

Figure

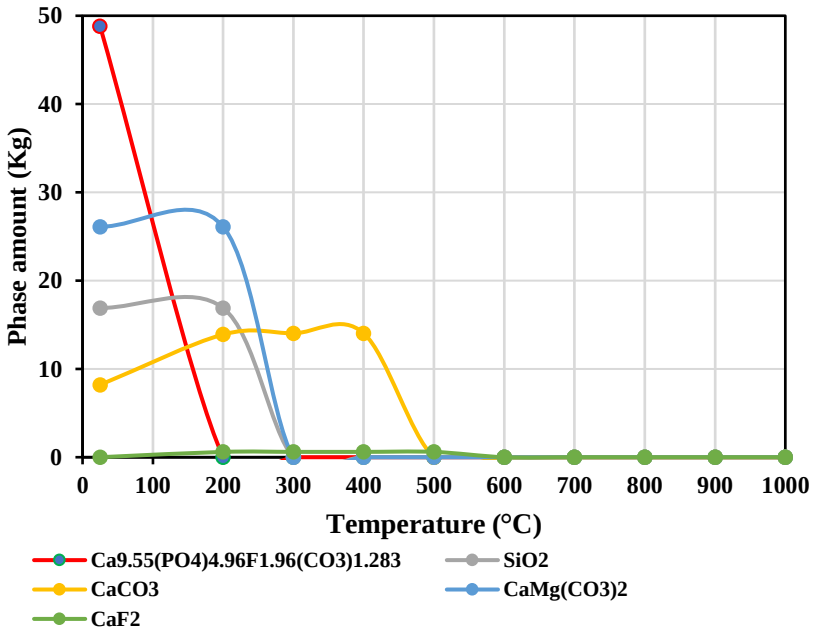

4-4 Conversion of minerals of low-grade phosphate ore and evolution of associated products at atmospheric equilibrium conditions (Part 1)

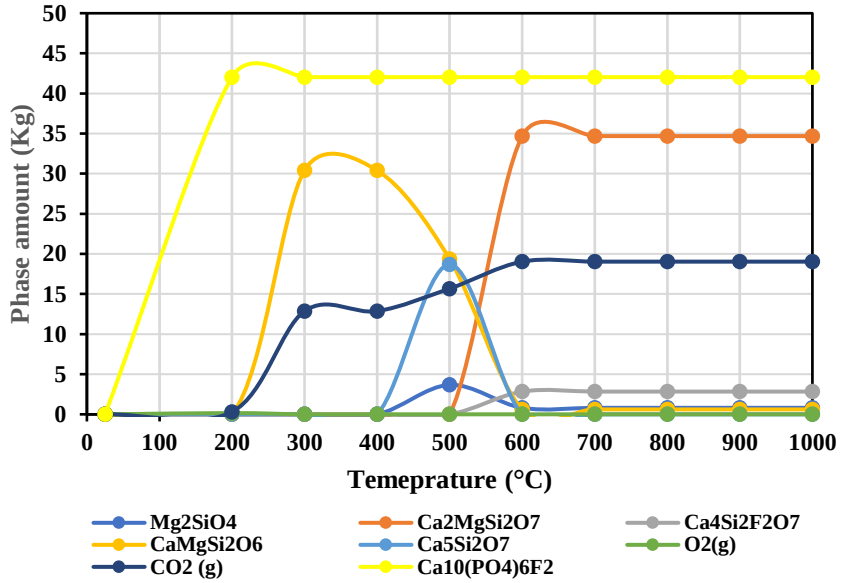

Figure 4-5 Phase distribution during thermal decarbonization of low-grade phosphate ore under equilibrium conditions (Part 2)

4.2.2 Thermal behaviour of individual minerals forming low-grade phosphate ore

The thermodynamic analysis of thermal behaviour of low-grade phosphate ore helped identify some products that could not be detected by XRD. Since the ore composed of several minerals, it was decided to evaluate the thermal behavior of each mineral separately for a better understanding of the interaction between minerals and its impact on the production of products during decarbonization. Hence, Factsage was employed to investigate the thermal behaviour of individual minerals.

$Ca_{9.55}(PO_4)_{4.96}F_{1.96}(CO_3)_{1.283}$ firstly decomposed at 200 °C into $Ca_{10}(PO_4)_6F_2$, CaF_2, CO_2, and $CaCO_3$, which then dissociates through a subsequent step into CaO and CO_2 (Figure 4-6 a). The thermal behaviour of $Ca_{9.55}(PO_4)_{4.96}F_{1.96}(CO_3)_{1.283}$ is not affected by the thermodynamic approach since it $Ca_{9.55}(PO_4)_{4.96}F_{1.96}(CO_3)_{1.283}$ decomposed at the same temperatures and $Ca_{10}(PO_4)_6F_2$ remained stable. However, decomposition temperature of formed $CaCO_3$ is affected by the

approach. This approach suggested that $CaCO_3$ completely decomposed at 900 °C, which agrees with XRD analysis.

At 500 °C, $CaMg(CO_3)_2$ is decomposed into MgO, CO_2, and $CaCO_3$, which then dissociated into CaO and CO_2 at 900 °C (Figure 4-6 b). This approach describes accurately behaviour of $CaMg(CO_3)_2$ suggested by XRD. While the former approach demonstrated that $CaMg(CO_3)_2$ completely reacted with SiO_2 at 300 °C.

Free $CaCO_3$ decomposed into CaO and CO_2 at 900 °C (Figure 4-16 c). The theoretical temperature predicted by Factsage for decomposition of $CaCO_3$ agrees with the experimental temperature suggested by XRD.

SiO_2 does not undergo any transformations at the studied temperatures when it is not associated with any phase (Figure 4-16 d).

CaO formed from decomposition of $Ca_{9.55}(PO_4)_{4.96}F_{1.96}(CO_3)_{1.283}$, $CaMg(CO_3)_2$, and $CaCO_3$ may react with SiO_2 at a specific molar fraction $SiO_2/(CaO+SiO_2)$ ranging between 0 and 0.35 to form dicalcium silicates (Ca_2SiO_4). The presence of Ca_2SiO_4 was confirmed by XRD at 800 °C for 40 min. In its turn, MgO generated from the decomposition of $CaMg(CO_3)_2$ can react with CaO and SiO_2 at specific ratios. However, XRD detected $CaMgSi_2O_6$ and Mg_2SiO_4 at 700 °C and 40 min.

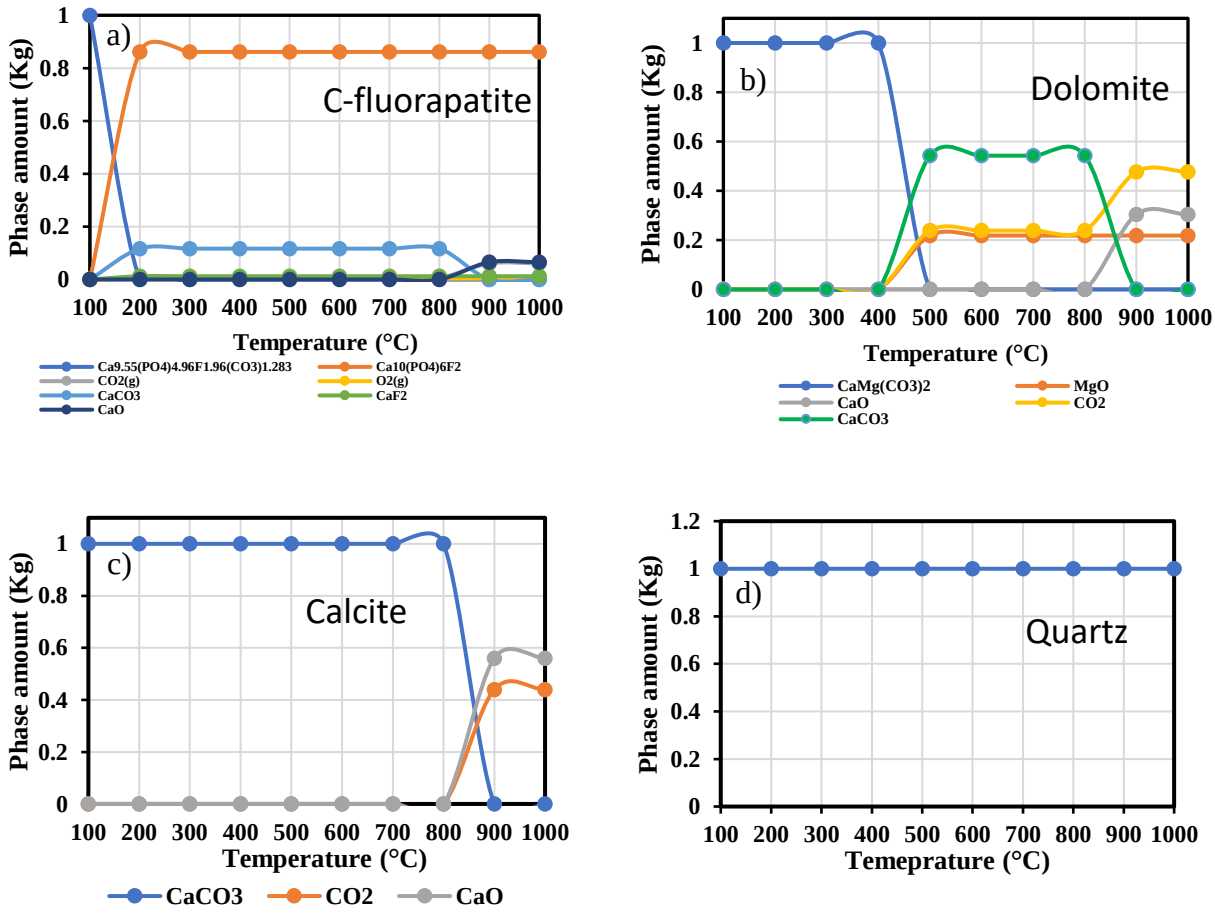

Figure 4-6 Thermal behaviour of individual minerals forming low-grade phosphate ore: a) C-fluorapatite, b) Dolomite, c) Calcite, d) Quartz

CHAPTER 5 KINETICS OF THERMAL DECARBONIZATION OF LOW-GRADE PHOSPHATE ORE

5.1 Thermogravimetric analysis of thermal behaviour of low-grade phosphate ore

Figures 5-1 and 5-2 present thermogravimetric (TG) and derivative thermogravimetric (DTG) curves of phosphate ore decarbonization at four heating rates of 2, 4, 8, and 20 °C/min. DTG curves shift toward higher temperatures when the heating rate increase, causing heat transfer limitations. The overall mass loss between room temperature and 1000 °C is quite similar, i.e., 20.48-23.34 %, at various rating rates. The insignificant discrepancy of overall mass loss according to the heating rate may be attributed to the thermal lag, which becomes significant as the heating rate increases, resulting in an incomplete decomposition of a specific component. The compositional heterogeneity of samples may also result in a difference in mass loss.

The decomposition reaction rate depicted in DTG curves shows two overlapped peaks at heating rates 2, 4, and 8 °C/min. However, it is difficult to visualize two separated peaks at 20 °C/min, but the DTG profile shows the first peak with a strong decomposition reaction rate linked to a shoulder peak. The DTG curves demonstrate that the thermal behaviour of phosphate ore is similar regardless of the heating rate. The temperatures and rates corresponding to the highest mass loss of each peak as a function of the heating rate are summarized in Table 5-1. Furthermore, TG curves of mass loss demonstrated the existence of two sigmoidal curves at 2, 4, and 8 °C/min (circled zone). This suggests that thermal decarbonization of phosphate ore can be divided into two main steps.

The temperature range of individual steps is difficult to estimate from the curves due to the overlapping of DTG curves of corresponding peaks. The first step must be attributed to the

decomposition of carbonate minerals calcite and dolomite, while the second step must relate to the decomposition of carbonate-fluorapatite. The higher mass loss of the first step than the second step is due to the high concentration and dolomite. The first step with the stronger peak occurs in wider temperature than the second step. The detailed kinetic analysis will enable us to identify reactions of the thermal decarbonization of low-grade phosphate ore.

It is worth noting that a negligible mass loss of 2-3% is observed at lower temperatures (Room temperature-500 °C) than those of steps 1 and 2. This could be attributed to the removal of moisture and organic matter [56, 63]. It was discarded in our analysis because it was not within the scope of the present research study.

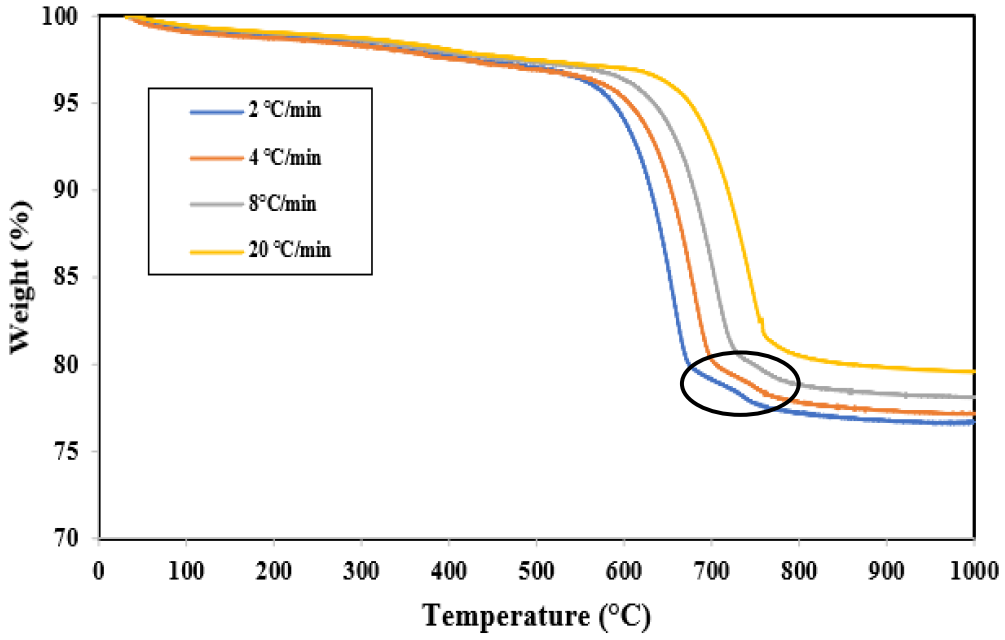

Figure 5-1 TG curves of thermal decarbonization of phosphate ore at different heating rates

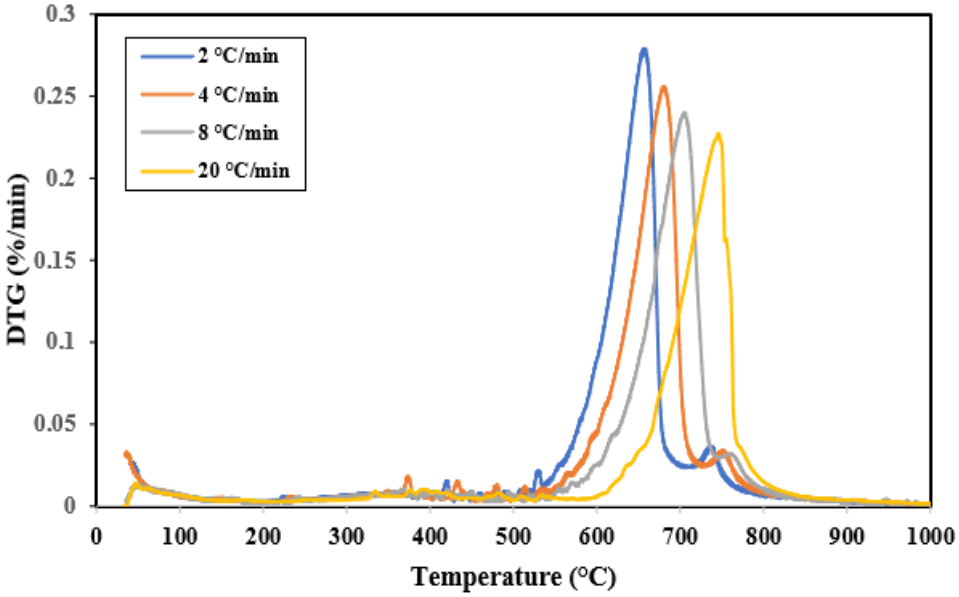

Figure 5-2 DTG curves of thermal decarbonization of phosphate ore at different heating rates

Table 5-1 T_{max} and $(dm/dt)_{max}$ of two peaks

Heating rate (°C/min)	Peak 1		Peak 2	
	T_{peak1}(°C)	$(dm/dt)_{peak1}$ (%/min)	T_{peak2}(°C)	$(dm/dt)_{peak2}$ (%/min)
2	660.21	0.2738	736.93	0.0345
4	683.63	0.251	758.12	0.0318
8	707.15	0.237	777.28	0.03144
20	749.21	0.221	-	-

Figure 5-3 illustrates the plots of conversion α calculated from Equation 9 versus T at different heating rates derived from mass loss between room temperature and 1000 °C. The temperature required to achieve a specific conversion increases when the heating rate rises. The appearance of

two S-shaped curves with two inflection points at 2, 4, and 8 °C/min in α-T plots confirm the complexity of thermal decarbonization of low-grade phosphate ore at T > 500 °C depending on the heating rate. α is required to conduct kinetic modeling of thermal decarbonization of low-grade phosphate ore.

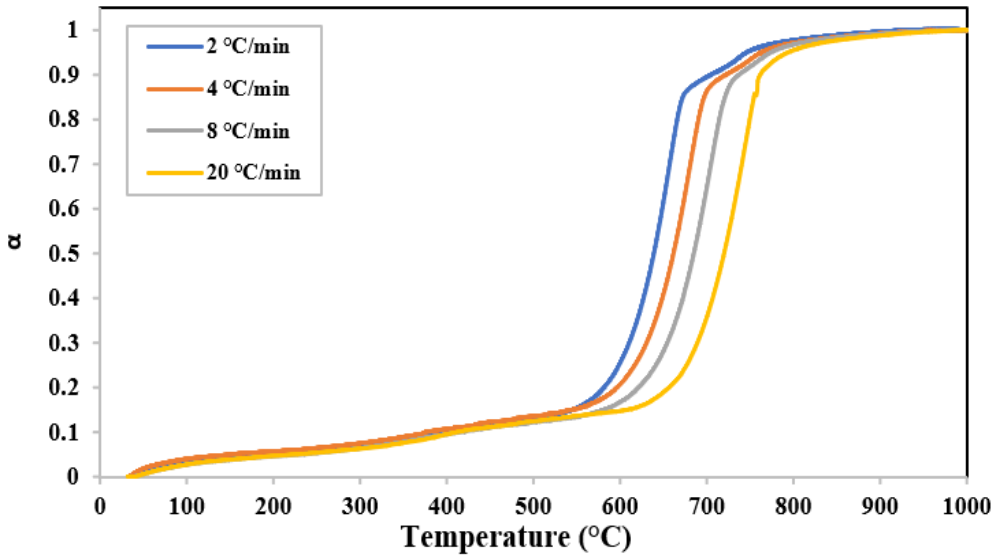

Figure 5-3 Conversion of thermal decarbonization of low-grade phosphate ore at different heating rates

5.2 Kinetics analysis

5.2.1 Isoconversional methods

Four isoconversional methods were applied at conversions between 0.2 and 0.9 with a step 0.1 to determine the distribution of activation energy of thermal decarbonization of low-grade phosphate ore. Figure 5-4 illustrates the isoconversional plots calculated from OFW (Equation 10), KAS (Equation 11), Starink (Equation 12), and Vyazovkin (Equation 13). The isoconversional plots are parallel between 0.2 and 0.8 for OFW, KAS and Starink, which means that they have similar slopes and thus provide the same activation energy. The isoconversional activation energy was derived

from the slops of the isoconversional plots of three methods OFW, KAS, and Starink. Vyazovkin method directly gives the isoconversional activation energy by minimizing the function depicted in Equation 13. The conversion dependence of activation energy for four isoconversional methods is shown in Figure 5-5. The variation of activation energy with conversion has a similar path for the four isoconversional methods despite the higher values calculated from OFW methods.

According to the change of activation energy versus conversion, isoconversional methods confirm that thermal decarbonization of phosphate ore is a complex process that can be classified into three steps rather than two steps as visualized from TG, DTG, and α plots. The inclusion of a hidden peak or a hidden shoulder peak within the main peak may explain why the visualization of a third peak from the DTG curve is difficult. This hidden peak may be attributed to the decomposition of magnesite. However, using the criteria of constancy of activation energy suggests three steps: 1) Ea =170.76-190.84 KJ/mole for the first step occurring at $0.2 \leq \alpha \leq 0.3$, 2) Ea =187.75-207.16 KJ/mole for the second step occurring at $0.3 < \alpha \leq 0.8$, 3) Ea =367.38-388.08 KJ/mole for the third step occurring at $0.8 < \alpha \leq 0.9$. The activation energy at conversion ranging between 0.2 and 0.9 using the four methods are summarized in Appendix A. The activation energies of steps 1 and 2 are quite similar and agree with those of thermal decomposition of calcite and dolomite obtained from literature (Tables 5-2, 5-3). The slight difference of activation energy calculated in the present research study and literature must be attributed to the procedural parameters and operational conditions (heating rate, TGA, sample size, particle size, composition of samples). Step 3 must be attributed to thermal decomposition of carbonate-fluorapatite. Ea=367.388 KJ/mole obtained in this research work is higher than that estimated by MattHews et al. [54], who found an activation energy of 261.25 KJ/mole for decarbonization of pure carbonate-fluorapatite.

Vyazovkin et al. [74] suggested a criterion to reveal the complexity of the process based on the isoconversional methods. They stated that the change of activation energy is insignificant when the lowest and highest values of activation energies are less than 10-20% of average activation energy [74]. This criterion can be helpful for an accurate selection of the number of steps in complex processes. This criterion is valid in the present research study since the difference according to the four isoconversional methods is within 10-20% at conversion range of 0.2-0.8: 11% for OFW, 12% for KAS, 11% for Starink, and 10% for Vyazovkin. Hence, we can assume that the reaction progress at α=0.2-0.8 corresponds to a single step rather than two steps. This hypothesis will be helpful to simplify the application of the Coats-Redfern method for model fitting methods. Assuming a single step in the range of 0.2-0.8 appears plausible because decomposition of dolomite and calcite has similar activations energies. The two possible steps are decomposition of magnesite into magnesium oxide and carbon dioxide and decomposition of calcite into calcium oxide and carbon dioxide. Although dolomite decomposes through two consecutive steps [74, 79, 80], most studies suggested that this overall transformation is represented by a single step at controlled reducing and oxidizing atmospheres [79-81]. Garcia et al. [82] found that the decomposition of both calcite and dolomite takes place in the same temperature range (540-650 °C). Furthermore, the activations energies of both transformations were quite similar for both decomposition of dolomite and calcite for each kinetic method [82].

This information supported our assumptions to consider a single step at conversion of 0.2-0.8 that corresponds to both decomposition of calcite and dolomite. The average activation of the first step (decomposition of calcite and dolomite) and second step (decomposition of carbonate fluorapatite) is summarized in Table 5-4.

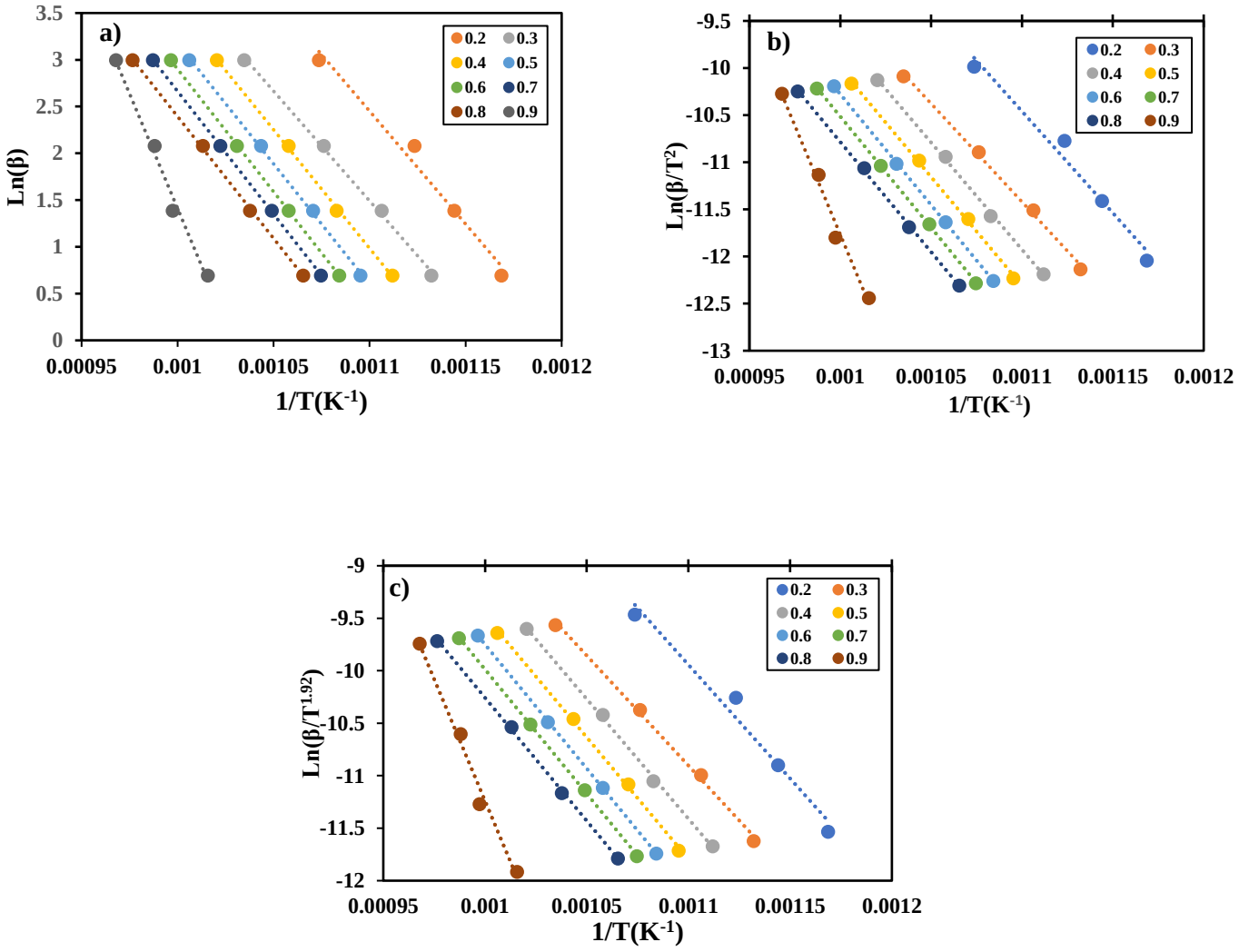

Figure 5-4 Isoconversional plots of thermal decarbonization of low-grade phosphate ore at 0.2-0.9: a) OFW, b) KAS, c) Starink

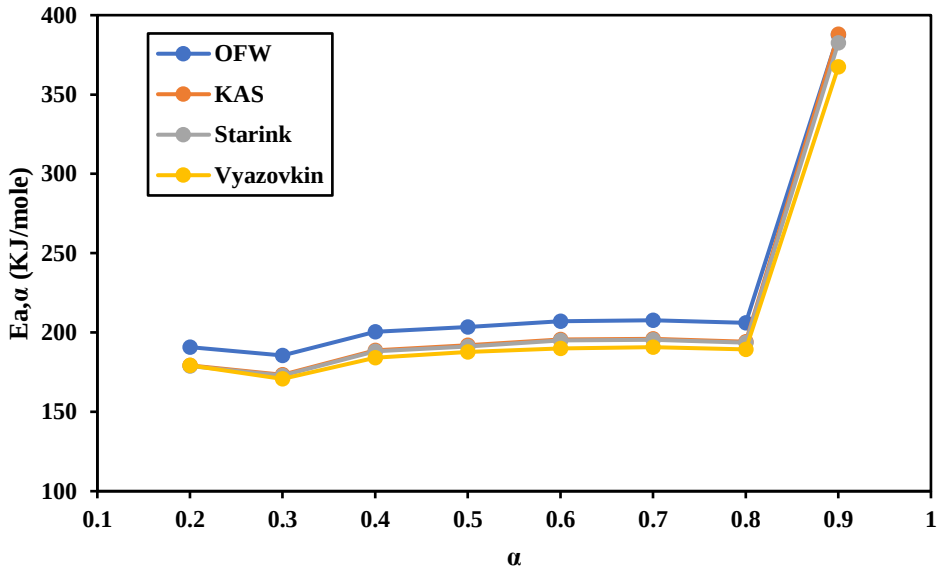

Figure 5-5 Variation of activation energy versus conversion using OFW, KAS, Starink and Vyazovkin methods

Table 5-2 Activation energies of thermal decomposition of calcite obtained by different studies

Sample	Method	$E_{a,\alpha}$ (KJ/mole)	Temperature range of step (°C)	Tpeak (°C)	Ref.
Natural $CaCO_3$	OFW, KAS	159.3-166.9	600-750 (12 K/min)	742.8 (12 K/min)	[83]
Synthetized $CaCO_3$	OFW, KAS	133.5-137.8	-	749.5 (12 K/min)	[83]
Standard $CaCO_3$	Vyazovkin	206-221	-	-	[84]
Pure $CaCO_3$ (200-500 µm)	Isoconversional and model fitting techniques	163.4-217.3	540-650	-	[82]
$CaCO_3$ (1.7-2 mm)	Model fitting	174	700-800	-	[85]

Table 5-3 Activation energies of thermal decomposition of dolomite obtained by different studies

Sample	Method	$E_{a,\alpha}$ (KJ/mole)	Temperature range of step (°C)	Ref.
Pure dolomite	Isoconversional and model fitting techniques	161.5-223.1	540-650	[82]
Dolomite (100-125 µm)	Modeling fitting	133	600-750 (12 K/min)	[86]
Dolomite (< 150 µm)	Model fitting	135.5	800-950	[87]
dolomite (1.7-2 mm)	,Model fitting	149	700-800	[85]
Magnesite	Model fitting	71.01-88.91	550-700	[88]
Magnesite	Model fitting	200 (TGA)	> 500	[81, 89]

Table 5-4 Average activation energies of thermal decarbonization of low-grade phosphate ore using Friedman, FWO, KAS, Starink and Vyazovkin methods

	OFW	KAS	Starink	Vyazovkin
E_{step1} (KJ/mole)	200.18	188.46	187.84	184.59
E_{step2} (KJ/mole)	387.60	388.08	382.60	367.38

5.2.2 Model fitting methods

Thermogravimetric analysis and isoconversional methods suggested that thermal decarbonization of phosphate ore involves two steps between 500 and 1000 °C. The application of model-fitting methods with the Coats-Redfern equation for multistep processes provides meaningless kinetic parameters which describe the kinetic behaviour of the overall progress rather than individual

steps. Hence, the Coats-Redfern equation is limited to processes characterized by a single step or a representative rate-limiting step having constant activation energy. To correctly apply Coat-Redfern, it is necessary to determine the contribution of each step on the mass loss i.e., conversion, and define the interval temperature of each step.

Prior to the use of model-fitting methods at a single heating rate of 2 °C/min, the dα/dT curve, i.e., reaction rate, of thermal decarbonization of phosphate ore was deconvoluted using Peak Fit software. Many studies recommended this preliminary procedure to improve the accuracy of kinetic analysis when dealing with multistep systems [90]. The asymmetric HVL (Haarhoff-Van der Linde) model was selected as the best multiple-peak fitting function to separate the overlapping peaks of total experimental dα/dT (Figure 5-6). dα/dT curve (Figure 5-6) was deconvoluted based on three criteria: i) The constancy of activation energy according to the conversion of the overall process using isoconversional methods (Figure 5-5), ii) deconvolution and curve-fitting of dα/dT plot with Peak Fit software, and iii) thermal and kinetic behaviour of dolomite and calcite discussed in the literature [81, 82, 86, 89]. The mathematical deconvolution validated the occurrence of two steps during thermal decarbonization of phosphate ore (Figure 5-6). The dα/dT curve was deconvoluted into two zones describing the progress of the two steps. The approximated onset temperature, offset temperature, and peak temperature are summarized in Table 5-5. The negligible residual sum of square (RSS= 0.0001875) and the high correlation coefficient (R^2=0.9928) showed the good fitting between experimental reaction rate $(d\alpha/dT)_{exp}$ and calculated reaction rate from the multiple peak model $(d\alpha/dT)_{calc}$.

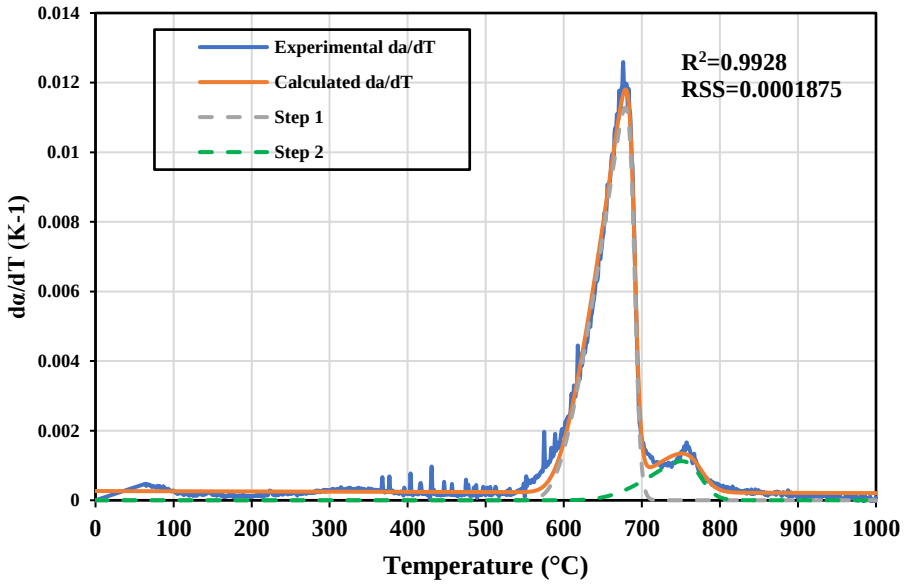

Figure 5-6 Deconvolution of dα/dT plots of thermal decarbonization of phosphate ore at 2 °C/min

Table 5-5 Limit temperatures of steps 1 and 2 at 2 °C/min

Parameter	Step 1	Step 2
T_{onset} (°C)	561.84	629.51
T_{peak} (°C)	681.02	751.14
T_{offset} (°C)	713.25	795.67

Two different techniques were used to determine the conversion of individual steps. The objective was to identify the reliable technique that gives comparable activation energy to that provided by isoconversional methods and literature data. Hence, isoconversional activation energy and

activation energy of pure-carbonate-fluorapatite decomposition obtained by MattHews et al. [54] were used as reference to compare the accuracy of both techniques.

Technique 1: To simplify the kinetic analysis, we discarded the interactions between the two overlapping peaks and considered that the corresponding steps proceeded as independent events in series without interactions. α-T curve at 2 °C/min depicted in Figure 5-3 was normalized between 500 and 760 °C. The first zone corresponds to the first step and ranges between 574-661 °C ($0.1 \leq \alpha \leq 0.8$) and the second region corresponds to the second step and is studied between 700-760 °C ($0.8 < \alpha < 1$). The temperature range of step 1 was chosen based on the results of previous studies [82] and variation of isoconversional activation energy conducted in the present study. The normalized conversion of both steps is illustrated in Figure 5-7. Coats-Redfern equation was then separately applied to estimate triple kinetic parameters (E_{a1}, A_1, $g_1(\alpha)$) and (Ea_2, A_2, $g_2(\alpha)$) of step 1 and step 2, respectively.

Technique 2: The reaction rates of individual steps obtained from mathematical deconvolution were integrated to derive the conversion of each step. The advantage of This technique is advantageous because it considers the interaction of both steps when they proceed in series in overlapping zone. Figure 5-8 shows that the conversion plot of each individual steps has single S-shaped curve confirming they are single steps. However, the integration may generate noisy data that can affect the accuracy of kinetics data. The onset and offset temperatures of both steps are those mentioned in Table 5-5. Coats-Redfern equation was then separately applied to estimate triple kinetic parameters (E_{a1}, A_1, $g_1(\alpha)$) and (Ea_2, A_2, $g_2(\alpha)$) of step 1 and step 2, respectively.

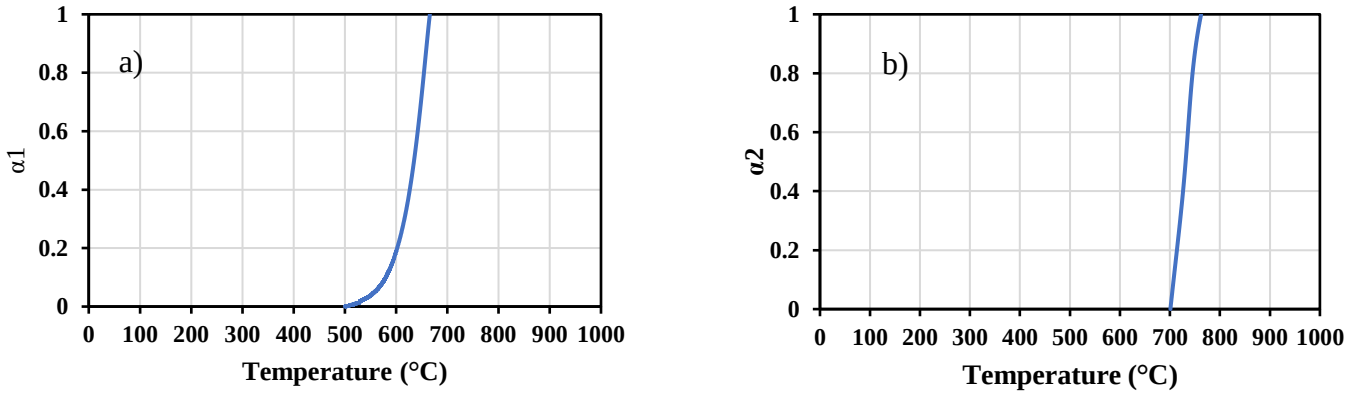

Figure 5-7 Normalized conversions without numerical integration (Technique 1): a) step 1, b) step 2

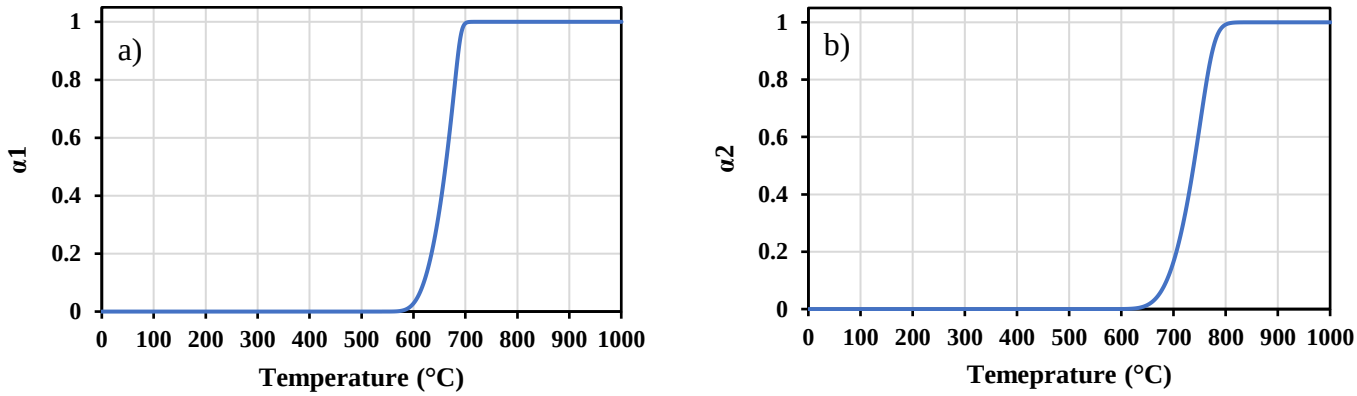

Figure 5-8 Normalized conversions with numerical integration of dα/dT of individual steps derived from deconvolution (Technique 1): a) step 1, b) step 2

5.2.2.1 Kinetic parameters of step 1

The most plausible solid-state kinetic models (Table 3-4) were tested to represent the progress of the first step. The selected appropriate kinetic model is the function that best fits the experimental data at 2 °C/min with the minimum residual sum of square value (RSS) using the Coats-Redfern equation. The kinetic parameters of the first step derived from different models are summarized in Table 5-6. For technique 1, R2, R3, and F1 models are the most appropriate models to describe

the kinetic behaviour of step 1 because their RSS range is between 0.84 and 7.17. Nevertheless, the contracting area model (R2) seems the most suitable mechanism model due to the lowest value of RSS=0.84. This model considers that the nucleation of the product on the surface of unshrunk particles is faster than shrinkage toward the center. However, this model was built for cylindrical particles. The sphericity of the particles of low-grade phosphate ore used in the present study was not measured. This uncertainty led to assume that the curve fitting does not guarantee that the selected kinetic model based on RSS is the most suitable function to describe the progress of reactions. The shape of particles may be changed during thermal treatment due to the agglomeration. This phenomenon could result in the formation of particles with the cylindrical form before decomposition began. However, we assume that R2 is the appropriate kinetic model with Ea=193.96 KJ/mole and A=2.62x10^9 s^{-1}. The calculated Ea agrees with those obtained from the four isoconversional methods 184.59-200.18 KJ/mole (Table 5-2) and those obtained by Garcia et al. [82] for decomposition of pure calcite (163.4-217.3 KJ/mole) and pure dolomite (161.5-223.1 KJ/mole) (Tables 5-3, 5-4). Figure 5-9 (a) depicts the Coats-Redfern plots of the validated kinetic model (R2) for technique 1 used to describe step 1 that includes decomposition of calcite and dolomite (Unified kinetic model of both transformations). The rate of step 1 with technique 1 can be written as follow:

$$\frac{d\alpha_1}{dt} = 2.62\text{x}10^9 e^{-\frac{193.96x10^3}{RT}}(2(1-\alpha_1)^{1/2}) \quad (18)$$

Technique 2 (numerical integration of deconvoluted dα/dT) confirmed that R2 and R3 are the best-fitting models for step 1 with close activation energy (Ea=229.52-257.76 KJ/mole) to the technique 1 and insignificant values of RSS=0.38-0.98 (Table 5-6). However, R2 was selected as the most probable kinetic model with Ea=229.52KJ/mole and A=1.24x$10^{11}$$s^{-1}$. Technique 1 provided Ea 15% less than technique 2, which can be acceptable as an error if we consider the slight difference

in temperature ranging and the technique used to determine α1. These results validate the reliability and applicability of the deconvolution procedure, corresponding multipeak fitting function selected and numerical integration of dα/dT of the individual step 1. Figure 5-9 (b) depicts the Coats-Redfern plots for the validated kinetic model (R2) of technique 2 used to describe step 1. The rate of step 1 for technique 2 can be written as follow:

$$\frac{d\alpha_1}{dt} = 1.24\text{x}10^{11} e^{-\frac{229.52x10^3}{RT}} (2(1-\alpha_1)^{1/2}) \quad (19)$$

Table 5-6 Kinetic parameters of first step at heating rate 2 °C/min for different kinetic models

Model	Technique 1			Technique 2		
	Ea(KJ/mole)	A (s^{-1})	RSS	Ea(KJ/mole)	A (s^{-1})	RSS
R2	193.96	$2.62\text{x}10^{9}$	0.84	229.52	$1.24\text{x}10^{11}$	0.96
R3	203.56	$6.92\text{x}10^{9}$	2.46	257.76	$3.84\text{x}10^{12}$	0.38
A2	249.05	$2.08\text{x}10^{13}$	433	256.11	$1.30\text{x}10^{13}$	12.19
A3	246.98	$1.84\text{x}10^{13}$	686	256.46	$1.39\text{x}10^{13}$	30.99
D1	265.65	$2.99\text{x}10^{13}$	159	273.61	$2.97\text{x}10^{13}$	18.56
D2	269.44	$2.96\text{x}10^{13}$	275	276.42	$2.99\text{x}10^{13}$	32.89
F1	220.85	$2.55\text{x}10^{11}$	7.17	262.78	$2.97\text{x}10^{13}$	7.37
F2	253.01	$2.99\text{x}10^{13}$	84	253.03	$2.95\text{x}10^{13}$	319

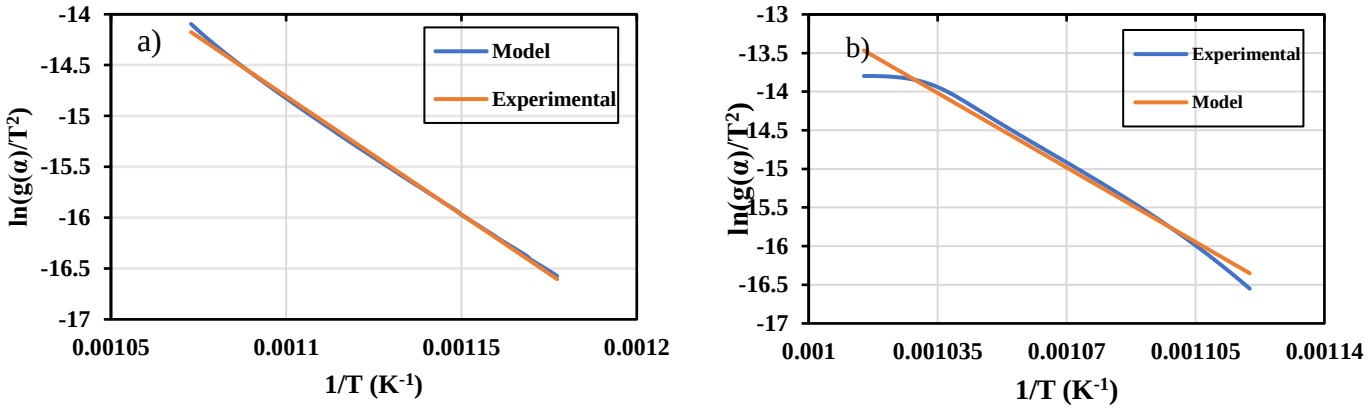

Figure 5-9 Coats-Redfern plot for step 1: a) Technique 1 (R2) b) Technique 2 (R2)

5.2.2.2 Kinetic parameters of step 2

Kinetic parameters of the second step were estimated in the same manner as the first step. For technique 1, the RSS criterion suggested that Avrami-Erofeev (RSS=0.78) is considered as the best fitting model to describe the progress of step 2. Hence, the activation energy of step 2 derived from the Avrami-Erofeev (A2) model is 239.99 KJ/mole, and the corresponding pre-exponential factor is 1.54×10^{11} s^{-1}(Table 5-7). The reaction shift from the R2 model for step 1 to the A2 model for step 2 is resealable. Avrami-Erofeev was constructed to illustrate the phase transformations from a state to another. If we assume that step 2 corresponds to the decomposition of carbonate-fluorapatite into carbon dioxide and fluorapatite, we then recognize the recrystallization of the structure of carbonate-fluorapatite to form fluorapatite. Hence, the atomic rearrangement during the decomposition is may be the rate-limiting step of this transformation. For technique 2, the appropriate kinetic model is the first-order reaction model (F1) that governs step 2 based on the RSS criterion. The activation energy derived from the F1 model is 265.76 KJ/mole, and the corresponding pre-exponential factor is 2.44×10^{12} s^{-1}. As a reminder, the conversion data in this

technique was derived from deconvolution of dα/dT. Despite the difference in representing the reaction model for techniques 1 and 2, both techniques provided quite a similar activation energy and pre-exponential factor. Activation energy obtained through technique 1 is 9.6% less that that of technique 2. This coherence neglects the effect of interactions between overlapping peaks on the evaluation of kinetic parameters.

The source of significant deviation of activation energy of step 2 between isoconversional methods (367.38-388.08 KJ/mole) and model fitting methods (239.99-265.76 KJ/mole) is not obvious. However, the activation energy obtained from model-fitting methods for step 2 (239.99-265.76 KJ/mole) is comparable to the activation energy obtained by MattHews et al. [54], who found that the activation energy of decarbonization of pure carbonate-fluorapatite is 261.25 KJ/mole. This coherence validates the reliability of the mathematical deconvolution approach, selected multipeak fitting function, and accuracy of techniques 1 and 2 for determination of α_2 (particularly technique 2).

The rate of step 2 for technique 1 can be written as follow:

$$\frac{d\alpha_2}{dt} = 1.54\text{x}10^{11} e^{-\frac{239.99x10^3}{RT}} (2(1-\alpha_2)[-\ln(1-\alpha_2)]^{1/2} \quad (20)$$

The rate of step 2 for technique 1 can be written as follow:

$$\frac{d\alpha_2}{dt} = 2.44\text{x}10^{12} e^{-\frac{265.76x10^3}{RT}} (1-\alpha_2) \quad (21)$$

Table 5-7 Kinetic parameters of second step at heating rate 2 °C/min for different kinetic models

Model (Table 3-4)	Technique 1			Technique 2		
	Ea(KJ/mole)	A (s^{-1})	RSS	Ea(KJ/mole)	A (s^{-1})	RSS
R2	290.87	$2.96x10^{13}$	8.31	291.28	$1.70x10^{13}$	40.52
R3	293.84	$2.95x10^{13}$	55.04	296.04	$2.27x10^{13}$	27.79
A2	239.99	$1.54x10^{11}$	0.78	283.86	$2.08x10^{13}$	71.16
A3	275.93	$1.22x10^{13}$	30.79	281	$1.45x10^{13}$	117.11
D1	291.55	$2.96x10^{13}$	130.90	274.48	$1.70x10^{12}$	26.88
D2	294.39	$2.99x10^{13}$	224.22	300.98	$2.95x10^{13}$	26.43
F1	282.40	$2.99x10^{13}$	94.83	265.76	$2.44x10^{12}$	0.27
F2	274.71	$2.95x10^{13}$	1179	274.87	$2.99x10^{13}$	347.50

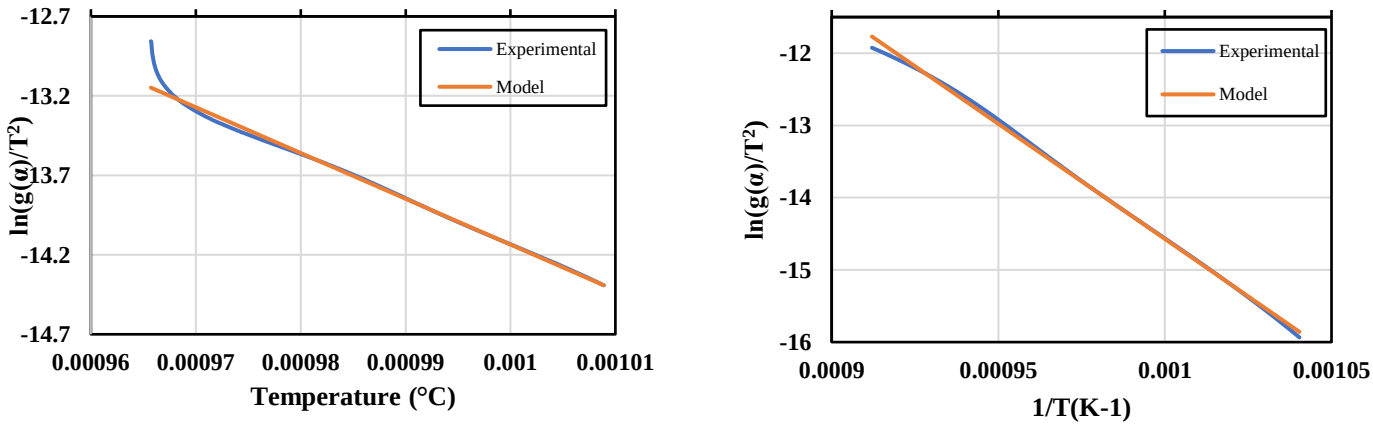

Figure 5-10 Coats-Redfern plot for step 1: a) Technique 1 (A2) b) Technique 2 (F1)

CHAPTER 6 REACTION PATHWAY OF THERMAL DECARBONIZATION OF LOW-GRADE PHOSPHATE ORE

By combining phase transformation provided by XRD and thermodynamic analysis with Factsage and kinetic analysis with thermogravimetry, the following reaction scheme is proposed during the decarbonization process:

❖ **Decomposition of individual minerals**:

$$CaMg(CO_3)_2(s) \rightarrow CaCO_3(s) + MgO(s) + CO_2(g) \quad (22.a)$$

$$CaCO_3(s) \rightarrow CO_2(g) + CaO(s) \quad (22.b)$$

$$CaMg(CO_3)_2(s) \rightarrow CaO(s) + MgO(s) + 2CO_2(g) \quad (22.c)$$

$$CaCO_3(s) \rightarrow CO_2(g) + CaO(s) \quad (23)$$

$$Ca_{9.55}(PO4)_{4.96}F_{1.96}(CO_3)_{1.283} \rightarrow 0.826Ca_{10}(PO4)_6F_2 + 0.153CO_2(g) + 0.153CaF_2 + 1.13CaCO_3 + 0.0765O_2(g) \quad (24.a)$$

$$CaCO_3(s) \rightarrow CO_2(g) + CaO(s) \quad (24.b)$$

$$Ca_{9.55}(PO4)_{4.96}F_{1.96}(CO_3)_{1.283} \rightarrow 0.826Ca_{10}(PO4)_6F_2 + 1.283CO_2(g) + 0.153CaF_2 + 1.13CaO(s) + 0.0765O_2(g) \quad (24.c)$$

❖ **Solid-solid reactions:**

$$SiO_2(s) + 2MgO(s) \rightarrow Mg_2SiO_4(s) \quad (25)$$

$$2SiO_2(s) + CaO(s) + MgO(s) \rightarrow CaMgSi_2O_6(s) \quad (26)$$

$$SiO_2(s) + 2CaO(s) \rightarrow Ca_2SiO_4(s) \quad (27)$$

The thermal decarbonization of low-grade phosphate ore involves a complex mechanism that includes the decomposition of some individual initial minerals ($Ca_{9.55}(PO_4)_{4.96}F_{1.96}(CO_3)_{1.283}$, $CaCO_3$ and $CaMg(CO_3)_2$) that are not stable thermodynamically at the tested temperature range and solid-solid reactions without gas release. Firstly, $CaCO_3$ and $CaMg(CO_3)_2$) are decomposed into their metal oxides (CaO and MgO) and CO_2 (Equations 22a-b-c, Equation 23). Based on XRD analysis, these reactions were complete at 800 ºC. Then, $Ca_{9.55}(PO_4)_{4.96}F_{1.96}(CO_3)_{1.283}$ dissociates into $Ca_{10}(PO_4)_6F_2$, CaF_2, CaO CO_2, and probably O_2, according to the global Equation 24-c. The formation of an amorphous CaF_2 or a crystalline CaF_2 with undetectable concentration are among the possible reasons for the non-detection of CaF_2 with XRD. This reaction can result from the combination of two series/parallel reactions according to XRD analysis and thermodynamic modeling (Equations 24-a, 24-b). Moreover, the sharp increase of intensity between 800 and 900 ºC at 31.83º, 53.83º and 37.36º corresponding to CaO can validate that $CaCO_3$ is formed from decomposition of $Ca_{9.55}(PO_4)_{4.96}F_{1.96}(CO_3)_{1.283}$ according to Equation 24-a and then dissociates into CaO and CO_2 according to Equation 24-b. This explanation is valid if the other crystalline phases (Mg_2SiO_4, Ca_2SiO_4) sharing the same peak position (2θ) do not contribute significantly in the increase of this intensity since there is decrease of intensity of SiO_2 at 2θ=20.86º and 2θ=26.618º between 800 and 900 ºC for 40 min. However, mathematical deconvolution and kinetic modeling suggested that the overall reaction of decomposition of $Ca_{9.55}(PO_4)_{4.96}F_{1.96}(CO_3)_{1.283}$ can be represented by a single step that may be assumed as the rate-limiting step although both reactions (Equations 24-a, 24-b) contribute to the release of CO_2. Therefore, decomposition of $Ca_{9.55}(PO_4)_{4.96}F_{1.96}(CO_3)_{1.283}$ to form $Ca_{10}(PO_4)_6F_2$ (Equation24-a) seems more difficult to achieve compared to the simple decomposition of $CaCO_3$ and $CaMg(CO_3)_2$ because it involves

recrystallization to form $Ca_{10}(PO_4)_6F_2$. Lastly, decomposition of $Ca_{9.55}(PO_4)_{4.96}F_{1.96}(CO_3)_{1.283}$ was assumed to take place between 800 and 900 ºC according to XRD analysis.

The solid-solid interactions, which can not be validated by TGA due to the complexity of the process, are the second type of reactions in thermal decarbonization of low-grade phosphate ore. According to XRD and thermodynamic analyses, most products formed from the decomposition of the components of low-grade phosphate ore act as intermediate products if they bind with SiO_2 at a proper molar ratio to form calcium silicate minerals, calcium silicate magnesium phases, and magnesium silicate phases. MgO released from the decomposition of $CaMg(CO_3)_2$ interacts with SiO_2 at a molar ratio of 2:1 to form Mg_2SiO_4 (Equation 25). XRD confirmed the presence of Mg_2SiO_4 at 700-900 ºC and equilibrium calculations validated its stability. $CaMgSi_2O_6$ formation is resulted from interaction between CaO, MgO and SiO_2 with a molar ratio of CaO:MgO:SiO_2 of 1:1:2 (Equation 26). XRD confirmed the presence of $CaMgSi_2O_6$ at only 700 ºC. The thermodynamic analysis validated the feasibility of the reaction depicted in Equation 26.

In its turn, Ca_2SiO_4 was formed from the interaction of SiO_2 and CaO generated from decomposition of carbon-bearing minerals (Equation 27). This reaction takes place at a molar ratio of SiO_2:CaO of 1:2 between 800 and 900 ºC for 40 min. however, a strong rise of intensity at $2\theta=37.36º$ corresponding to Ca_2SiO_4 and other crystalline phases in XRD patterns was observed at 900 ºC. This increase was compensated by a sharp decrease of intensity of SiO_2 at $2\theta=20.86º$ and $2\theta=26.618º$ at the same temperature. The approach 1 of thermodynamic analysis showed the formation of $Ca_5Si_2O_4$. However, XRD and approach 2 of thermodynamic analyses confirmed the formation of Ca_2SiO_4. The presence of whether $Ca_5Si_2O_4$ or Ca_2SiO_4 must depend on the molar ratio of SiO_2:CaO and the rate of their formation.

CONCLUSION

The present study provided an excellent opportunity to beneficiate low-grade phosphate ore by thermal treatment route to ensure performant and cost-effective operation of the smelting process. The obtained results provided a good understanding of the thermal behaviour of low-grade phosphate ore, which contains carbonate-fluorapatite as a phosphorus-bearing mineral, but also calcite, dolomite, and quartz. These accessory minerals also exhibit transformations during the process making the process more complex.

The few kinetics studies performed for thermal decomposition of phosphate ore in literature and the influence of various factors (sample size, mineralogy of phosphate ore, distribution of minerals, heating rate, particle size) encouraged us to construct a plausible reaction pathway and study the kinetics of low-grade phosphate ore thermal decarbonization with thermogravimetry.

Although widely studied in the literature, the thermal and kinetics behaviours of calcite and dolomite, as carbon-bearing minerals, were revealed by Factsage, XRD, and kinetic modeling. In addition, the present study threw light on the thermal and kinetic behaviour of carbonate fluorapatite, which also released carbon in the form of carbon dioxide and revealed its interactions with other minerals during the process.

The outcomes of the present study stimulated the adoption of thermal decarbonization as a successful pre-treatment step of the smelting process. However, more experimental works at the lab scale are recommended to study the kinetics of solid-solid reactions to mitigate uncertainties during scaling-up. Moreover, the change of specific surface area of decarbonized phosphate must be controlled to ensure good contact with reducing agents during the smelting process.

REFERENCES

1. Paytan, A. and K. McLaughlin, *The Oceanic Phosphorus Cycle*. Chemical Reviews, 2007. **107**(2): p. 563-576.
2. Geissler, B., M.C. Mew, and G. Steiner, *Phosphate supply security for importing countries: Developments and the current situation.* Science of The Total Environment, 2019. **677**: p. 511-523.
3. Cordell, D., J.-O. Drangert, and S.J.G.e.c. White, *The story of phosphorus: global food security and food for thought.* Global environmental change, 2009. **19**(2): p. 292-305.
4. Rulis, P., L. Ouyang, and W.J.P.R.B. Ching, *Electronic structure and bonding in calcium apatite crystals: Hydroxyapatite, fluorapatite, chlorapatite, and bromapatite.* Physical Review B, 2004. **70**(15): p. 155104.
5. *Mineral Resource of the Month: Phosphate Rock* *https://www.earthmagazine.org/article/mineral-resource-month-phosphate-rock/*
6. Kovler, K. and M. Somin. *Producing environment-conscious building materials from contaminated phosphogypsum*. in *Proceedings of the RILEM International Symposium on Environment-conscious Materials and Systems for Sustainable Development(ECM 2004), Koriyama, Japan*. 2004.
7. Ando, J.J.P.C.i.F.P., *Phosphoric Acid by Wet Process: Phosphogypsum, Transport, Storage, and.* Pollution Control in Fertilizer Production, 1994: p. 209.
8. Kouzbour, S., et al., *Comparative analysis of industrial processes for cadmium removal from phosphoric acid: A review.* Hydrometallurgy, 2019. **188**: p. 222-247.
9. Abouzeid, A.-Z.M., *Physical and thermal treatment of phosphate ores — An overview.* International Journal of Mineral Processing, 2008. **85**(4): p. 59-84.
10. López, F., et al., *Thermal dehydration kinetics of phosphogypsum.* Materiales de Construcción, 2015. **65**(319): p. 061.
11. Environment Protection Agency, U.E., *Source category survey : Thermal Process Phosphoric Acid Manufacturing Industry* 1980.
12. *Phosphorus in industry and society* https://phosphorusplatform.eu/images/download/ESPP%20conference%20Phosphorus%20stewardship/Schipper-ESPP-1-12-16.pdf.
13. Leder, F., et al., *Reduction of phosphate ore by carbon: Part II. Rate limiting steps.* Metallurgical Transactions B, 1986. **17**(4): p. 869-877.
14. Li, Y., et al., *Studies on extraction of phosphorus from phosphate ore by electric furnace with different fluxing agents.* Phosphorus, Sulfur, and Silicon and the Related Elements, 2018. **193**(3): p. 141-148.
15. Hussein, M., et al., *Kinetics of calcium phosphate reduction by carbon.* Thermochimica Acta, 1974. **10**(2): p. 177-186.

16. Cao, R., et al., *NiSO4 as Additive Effect on the Carbothermal Reduction Process of Phosphate Rock and SiO2.* Silicon, 2019. **11**(6): p. 2829-2836.

17. Sun, Y., et al., *Effect of different additives on reaction characteristics of fluorapatite during coal-based reduction of iron ore.* Metals, 2019. **9**(9): p. 923.

18. Dresen, C., et al., *Optimisation of pellet reduction in a phosphorus furnace.* Fundamentals of advanced materials for energy conversion. Extraction and Processing Division, The Minerals, Metals and Materials Society-TMS, Warendale, Pennsylvania, 2002: p. 435-447.

19. Li, Y., et al., *Study of the Silica or K-feldspar as fluxing agent for the yellow phosphorus production.* Phosphorus, Sulfur, and Silicon and the Related Elements, 2018. **193**(8): p. 520-527.

20. Chen, Z., Y. Li, and J.J.S. Xia, *Silica, Alkali Carbonate and Alkali Rich Metal Ore as Additive Effect on the Carbothermic Reduction Process of Phosphorus Ore.* Fundamentals of advanced materials for energy conversion. Extraction and Processing Division, The Minerals, Metals and Materials Society-TMS, Warendale, Pennsylvania, 2020. **12**(3): p. 613-620.

21. Zheng, G., et al., *The additive effect of K 2 CO 3-NiSO 4 on the carbothermal reduction process of phosphate rock and SiO 2.* Silicon 2020. **12**(8): p. 1985-1994.

22. PECHKOVSKII, V., et al., *REDUCTION OF CALCIUM PHOSPHATES IN PRESENCE OF SILICA.* 1985. **58**(12): p. 2433-2436.

23. Ding, B., et al., *Phase Change Cooling and Crystallization Characteristics of Blast Furnace Slags with Various MgO/Al2O3 Ratios.* Energy & Fuels, 2017. **31**(9): p. 10212-10221.

24. Zhang, Y., et al., *Phosphorus-containing mineral evolution and thermodynamics of phosphorus vaporization during carbothermal reduction of high-phosphorus iron ore.* Metals 2018. **8**(6): p. 451.

25. Leder, F., et al., *New process for technical-grade phosphoric acid.* Industrial & Engineering Chemistry Process Design and Development, 1985. **24**(3): p. 688-697.

26. Jacob, K., et al., *Reduction of tricalcium phosphate by carbon.* Industrial & Engineering Chemistry, 1929. **21**(11): p. 1126-1132.

27. Xia, J., R. Geng, and Z. Chen, *The Effect of K-feldspar and Silica as Fluxing Agent on the Production Process of Phosphorus Furnace.* Silicon, 2019. **11**(1): p. 233-239.

28. Kang, M.X., H.Y. Tian, and Y.X. Wu. *Study on Thermal Reduction of Phosphate Ore by carbon in the Fluidized Bed Reactor*. in *Advanced Materials Research*. 2012. Trans Tech Publ.

29. Mu, J., et al., *Reduction of phosphate ores by carbon: Part I. Process variables for design of rotary kiln system.* Metallurgical Transactions B, 1986. **17**(4): p. 861-868.

30. Hernáinz, F., M. Calero, and G. Blázquez, *Flotation of low-grade phosphate ore.* Advanced Powder Technology, 2004. **15**(4): p. 421-433.

31. Kawatra, S.K. and J. Carlson, *Beneficiation of phosphate ore*. 2013: Society for Mining, Metallurgy, and Exploration.

32. Abanades, S. and L. André, *Design and demonstration of a high temperature solar-heated rotary tube reactor for continuous particles calcination.* Applied Energy, 2018. **212**: p. 1310-1320.

33. Al-Fariss, T.F., H.O. Ozbelge, and H.S. El-Shall, *On the Phosphate Rock Beneficiation for the Production of Phosphoric Acid in Saudi Arabia.* Journal of King Saud University - Engineering Sciences, 1992. **4**(1): p. 13-31.

34. Valverde, J.M., et al., *Thermal decomposition of dolomite under CO2: insights from TGA and in situ XRD analysis.* Physical Chemistry Chemical Physics, 2015. **17**(44): p. 30162-30176.

35. Rat'ko, A., et al., *Thermal decomposition of natural dolomite.* Inorganic Materials, 2011. **47**.

36. Speight, J.G., *Chapter 13 - Upgrading by Gasification*, in *Heavy Oil Recovery and Upgrading*, J.G. Speight, Editor. 2019, Gulf Professional Publishing. p. 559-614.

37. Mancuso, L. and S. Arienti, *3 - Petroleum coke (petcoke) and refinery residues*, in *Integrated Gasification Combined Cycle (IGCC) Technologies*, T. Wang and G. Stiegel, Editors. 2017, Woodhead Publishing. p. 121-144.

38. Freeman, H.P., J.H. Caro, and N. Heinly, *Fertilizer Materials, Effect of Calcination on Character of Phosphate Rock.* Journal of Agricultural and Food Chemistry, 1964. **12**(6): p. 479-486.

39. Scheepers, E., et al., *The development of a CFD model of a submerged arc furnace for phosphorus production.* 2006. **19**(10): p. 1115-1125.

40. Chaabouni, A., et al., *Thermal Decomposition Of Two Tunisian Natural Phosphates And Study Of Kinetic Decarbonation.* INTERNATIONAL JOURNAL OF SCIENTIFIC & TECHNOLOGY RESEARCH VOLUME 6.

41. Haseman, J.F., *Beneficiation of phosphate ore containing carbonates*. 1968, Google Patents.

42. Petersen, A., *Process for treating phosphate ore*. 1973, Google Patents.

43. Baumann, A.N., *Method for upgrading pebble phosphate*. 1969, Google Patents.

44. Angevine, P.A. and D.W. Leyshon, *Fluid bed calcination process*. 1977, Google Patents.

45. Bailliez, S. and A. Nzihou, *The kinetics of surface area reduction during isothermal sintering of hydroxyapatite adsorbent.* Chemical Engineering Journal, 2004. **98**(1): p. 141-152.

46. Champion, E.J.A.b., *Sintering of calcium phosphate bioceramics.* Acta biomaterialia, 2013. **9**(4): p. 5855-5875.

47. El Mokhtar, E.O., *Effect of temperature and residence time of calcination phosphate on the chemical reactivity: Application to the case of Bouchane phosphate (Morocco).* CiteSeerX logo, 2013.

48. Mgaidi, A., et al., *Chemical and structural changes of raw phosphate during heat treatment.* High Temperature Materials and Processes, 2004. **23**(3): p. 185-194.

49. Somers, N., et al., *Influence of dopants on thermal stability and densification of β-tricalcium phosphate powders.* Open Ceramics, 2021. **7**: p. 100168.

50. Zhou, F., et al., *Investigation of decomposition of dolomite and distribution of iodine migration during the calcination-digestion process of phosphate ore.* Hydrometallurgy, 2019. **188**: p. 174-181.

51. Chen, W., et al., *Temperature-related changes of Ca and P release in synthesized hydroxylapatite, geological fluorapatite, and bone bioapatite.* Chemical Geology, 2017. **451**: p. 183-188.

52. Elgharbi, S., K. Horchani-Naifer, and M. Férid, *Investigation of the structural and mineralogical changes of Tunisian phosphorite during calcinations.* Journal of Thermal Analysis and Calorimetry, 2015. **119**(1): p. 265-271.

53. Knubovets, R., et al., *Thermal transformations in phosphorites.* Journal of thermal analysis, 1997. **50**(1): p. 229-239.

54. Matthews, A. and Y.J.A.M. Nathan, *The decarbonation of carbonate-fluorapatite (francolite).* American Mineralogist, 1977. **62**(5-6): p. 565-573.

55. Tõnsuaadu, K., et al., *A review on the thermal stability of calcium apatites.* Journal of Thermal Analysis and Calorimetry, 2012. **110**(2): p. 647-659.

56. Banane, E., et al., *The kinetics of the thermal decomposition of natural moroccan and iraqi phosphates.* Thermochimica Acta, 1989. **152**(1): p. 115-123.

57. Liu, N.A. and W.C. Fan, *Critical consideration on the Freeman and Carroll method for evaluating global mass loss kinetics of polymer thermal degradation.* Thermochimica Acta, 1999. **338**(1): p. 85-94.

58. Bilali, L., et al., *Pyrolysis of the Moroccan (Youssoufia) rock phosphate.* Journal of Analytical and Applied Pyrolysis, 2002. **65**(2): p. 221-237.

59. Khan, I., et al., *The pyrolysis kinetics of the conversion of Malaysian kaolin to metakaolin.* Applied Clay Science, 2017. **146**: p. 152-161.

60. Lyon, R.E., et al., *Thermokinetic model of sample response in nonisothermal analysis.* Thermochimica Acta, 2012. **545**: p. 82-89.

61. Lin, Y.-C., et al., *Kinetics and Mechanism of Cellulose Pyrolysis.* The Journal of Physical Chemistry C, 2009. **113**(46): p. 20097-20107.

62. Trache, D., A. Abdelaziz, and B. Siouani, *A simple and linear isoconversional method to determine the pre-exponential factors and the mathematical reaction mechanism functions.* Journal of Thermal Analysis and Calorimetry, 2017. **128**(1): p. 335-348.

63. Naktiyok, J., et al., *Kinetics of thermal decomposition of phospholipids obtained from phosphate rock.* Fuel Processing Technology, 2013. **116**: p. 158–164.

64. Vyazovkin, S., et al., *ICTAC Kinetics Committee recommendations for performing kinetic computations on thermal analysis data.* Thermochimica Acta, 2011. **520**(1): p. 1-19.

65. Farjas, J. and P. Roura, *Isoconversional analysis of solid state transformations.* Journal of Thermal Analysis and Calorimetry, 2011. **105**(3): p. 757-766.

66. Aouad, A., et al., *Kinetic Aspect of Thermal Decomposition of Natural Phosphate and its Kerogen. Influence of heating rate and mineral matter.* Journal of Thermal Analysis and Calorimetry, 2002. **67**(3): p. 733.

67. Olson, C., *Pyrolysis process kinetics of phosphate rock in a rotary kiln*. 2005: The University of Utah.

68. Vyazovkin, S. and C.J.A.r.o.p.c. Wight, *Kinetics in solids.* Annual review of physical chemistry,, 1997. **48**(1): p. 125-149.

69. Bale, C.W., et al., *FactSage thermochemical software and databases — recent developments.* Calphad, 2009. **33**(2): p. 295-311.

70. *General Gibbs Minimization as an Approach to Equilibrium.* http://courses.washington.edu/mengr524/sp15/handouts/gibbs_min.pdf.

71. Connolly, J.A.D., *A primer in gibbs energy minimization for geophysicists.* Petrology, 2017. **25**(5): p. 526-534.

72. Privat, R., et al., *Teaching the Concept of Gibbs Energy Minimization through Its Application to Phase-Equilibrium Calculation.* Journal of Chemical Education, 2016. **93**(9): p. 1569-1577.

73. Deb, P., *Kinetics of Heterogeneous Solid State Processes*. 2013, New Delhi, INDIA: Springer (India) Private Limited.

74. Vyazovkin, S., et al., *ICTAC Kinetics Committee recommendations for analysis of multi-step kinetics.* Thermochimica Acta, 2020. **689**: p. 178597.

75. Vyazovkin, S.J.J.o.t.a. and calorimetry, *Advanced isoconversional method.* Journal of thermal analysis and calorimetry, 1997. **49**(3): p. 1493-1499.

76. Khawam, A. and D.R. Flanagan, *Solid-State Kinetic Models: Basics and Mathematical Fundamentals.* The Journal of Physical Chemistry B, 2006. **110**(35): p. 17315-17328.

77. El-Kherbawy, M., et al. *Chemical Characterization of Phosphate Rock Applied in Arid Region*. in *Middle East Journal of Agriculture Research*. 2014.

78. Srarfi, F., et al., *Stream sediments geochemistry and the influence of flood phosphate mud in mining area, Metlaoui, Western south of Tunisia.* Environmental Earth Sciences, 2019. **78**(6): p. 211.

79. Otsuka, R., *Recent studies on the decomposition of the dolomite group by thermal analysis.* Thermochimica Acta, 1986. **100**(1): p. 69-80.

80. Olszak-Humienik, M. and J. Możejko, *Kinetics of Thermal Decomposition of Dolomite.* Journal of Thermal Analysis and Calorimetry, 1999. **56**(2): p. 829-833.

81. An, P., et al., *Energy-saving strategy for a transport bed flash calcination process applied to magnesite.* Carbon Resources Conversion, 2021. **4**: p. 122-131.

82. García, A.C., M. Latifi, and J. Chaouki, *Kinetics of calcination of natural carbonate minerals.* Minerals Engineering, 2020. **150**: p. 106279.

83. Georgieva, V., L. Vlaev, and K. Gyurova, *Non-Isothermal Degradation Kinetics of CaCO₃ from Different Origin.* Journal of Chemistry, 2013. **2013**: p. 872981.

84. Wang, D., et al. *Calcite: Kinetics of Two-step Thermal Decomposition*. in *2nd Annual International Conference on Advanced Material Engineering (AME 2016)*. 2016. Atlantis Press.

85. Britton, H.T.S., S.J. Gregg, and G.W. Winsor, *The calcination of dolomite. Part I.—The kinetics of the thermal decomposition of calcite and of magnesite.* Transactions of the Faraday Society, 1952. **48**(0): p. 63-69.

86. Ble and Ž.D. Živković, *A new method for the determination of reaction kinetics from DTA and TG curves. Part II. Application of the method to the thermal decomposition of carbonates.* Thermochimica Acta, 1983. **60**(1): p. 69-76.

87. Kissinger, H.E., *Reaction Kinetics in Differential Thermal Analysis.* Analytical Chemistry, 1957. **29**(11): p. 1702-1706.

88. Hou, Q., et al., *Non-isothermal kinetic study of high-grade magnesite thermal decomposition and morphological evolution of MgO.* Int J Appl Ceram Technol, 2021. **18**(3): p. 765-772.

89. JIANG Weiwei, H.W., LIU Xuejing, HAN Zhannan, YUE Junrong, XU Guangwen, *Characteristic and kinetics of light calcination of magnesite in micro fluidized bed reaction analyzer.* CIESC Journal: p. 0-0.

90. Vyazovkin, S., et al., *ICTAC Kinetics Committee recommendations for analysis of multi-step kinetic.* Thermochimica Acta, 2020. **689**: p. 178597.

APPENDICE A ISOCONVERSIONAL ACTIVATION ENERGIES PROVIDED BY OFW, KAS, STARINK AND VYAZOVKIN

	OFW		KAS		Starink		Vyazovkin	
	Ea(Kj/mole)	R^2	Ea(Kj/mole)	R^2	Ea(Kj/mole)	R^2	Ea(Kj/mole)	$\phi(Ea)$
0.2	190.84	0.9809	179.35	0.976	178.784	0.9762	179.28	12.9565
0.3	185.55	0.9982	173.38	0.9976	172.8702	0.9976	170.76	12.91989
0.4	200.44	0.9993	188.83	0.9991	188.2197	0.9991	184.21	12.95529
0.5	203.54	0.999	191.91	0.9988	191.2715	0.9988	187.75	12.92515
0.6	207.16	1	195.58	0.9999	194.9254	0.9999	190.00	12.97124
0.7	207.68	0.9999	196.01	0.9999	195.3543	0.9999	190.83	12.95168
0.8	206.04	0.9995	194.15	0.9994	193.5067	0.9994	189.31	12.94611
0.9	387.60	0.9883	388.08	0.9869	382.609	0.987	367.38	13.07327